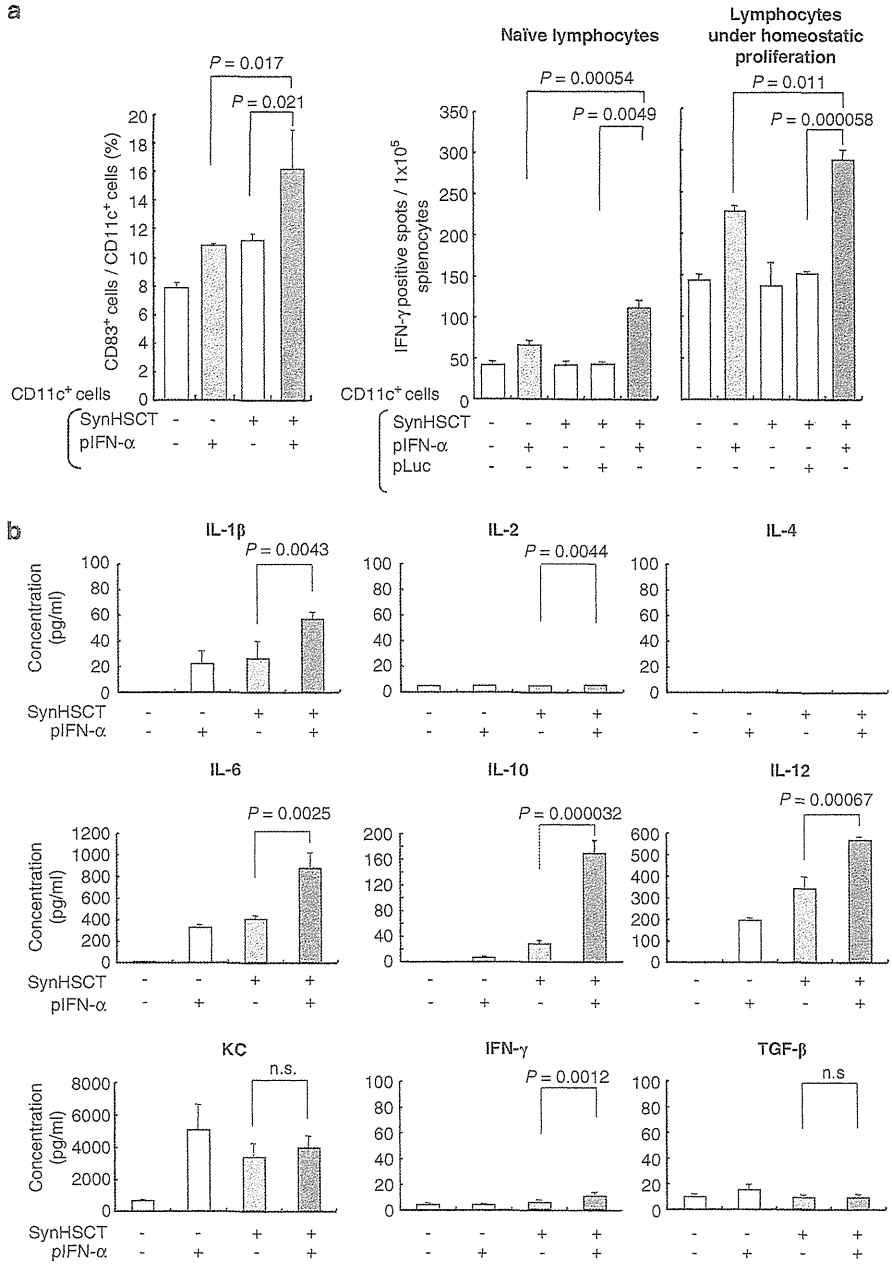

Figure 6 IFN-α expression promotes the maturation of CD11c$^+$ cells in the tumor. (**a**) Number of IFN-γ-positive cells by enzyme-linked immunosorbent spot assay. Flow cytometry of CD83$^+$ cells (Michel-19; BD Pharmingen) was performed in the CD11c$^+$ cells isolated from tumors (n=3). The frequency of CD83$^+$ cells per CD11c$^+$ cells is presented (left panel). CD11c$^+$ cells from treated tumors were co-cultured with lymphocytes isolated from naïve BALB/c mice (middle panel) or synHSCT mice (right panel), and lymphocyte activation was measured by IFN-γ-enzyme-linked immunosorbent spot assay (n=3). The experiments were repeated twice. (**b**) Cytokine production of CD11c$^+$ cells. CD11c$^+$ cells were isolated from treated tumors (n=3), and were seeded in a 48-well plate (1×10^5 cells per well). After the incubation for 48 h, cytokines in the medium were measured by a cytokine array (Procarta Cytokine Assay Kit; Panomics, Inc., Fremont, CA, USA). IL-10 level was measured by enzyme-linked immunosorbent assay (Quantikine; R&D Systems, Minneapolis, MN, USA). The experiments were repeated three times.

MATERIALS AND METHODS

Animals and hematopoietic stem cell transplantation

Seven-to-nine-week-old female BALB/c (H-2^d Ly-1.2) mice were purchased from Charles River Japan, Inc., (Kanagawa, Japan). Animal studies were carried out according to the *Guideline for Animal Experiments of the National Cancer Center Research Institute* and approved by the Institutional Committee for Ethics in Animal Experimentation. Nine-to-ten-week-old BALB/c mice received a lethal (9 Gy) irradiation on the day of transplantation. The irradiated BALB/c mice were injected intravenously with 5×10^6 of bone marrow cells and 2×10^6 splenic T cells from donor BALB/c mice. Bone marrow cells were isolated from donors by

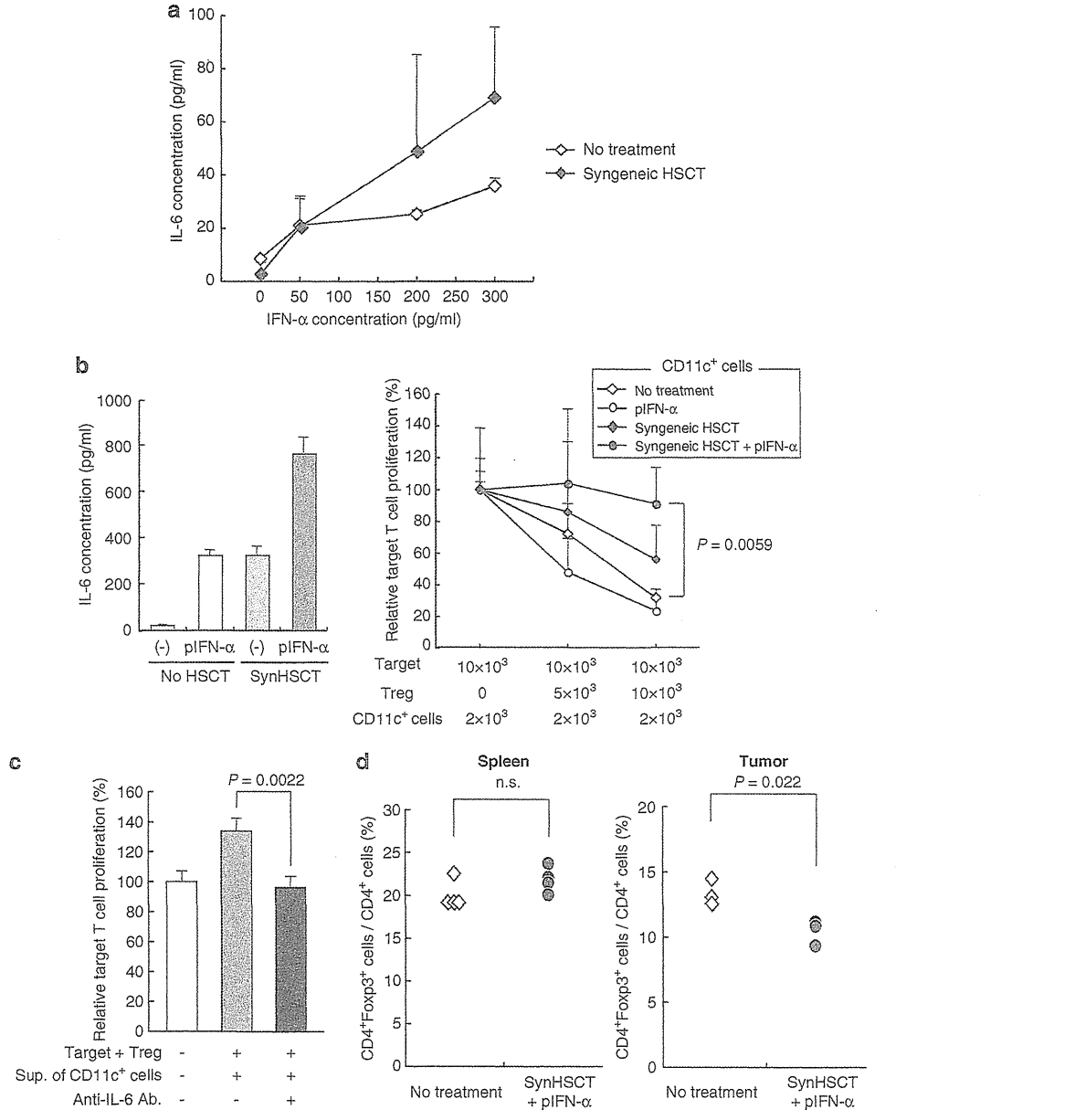

Figure 7 CD11c$^+$ cells in the tumor inhibit the immunosuppressive activity of Tregs. (**a**) CD11c$^+$ cells produce IL-6 in response to IFN-α. CD11c$^+$ cells isolated from the spleens of non-HSCT and synHSCT tumor-bearing BALB/c mice were seeded in a 96-well plate (1.5×10^5 cells per well) and cultured in the medium containing IFN-α protein at indicated concentration for 2 h. After the change of medium, the cells were incubated for 48 h, and IL-6 in the medium was measured by ELISA (Quantikine; R&D Systems). The experiments were repeated twice. (**b**) The inhibition of activity of Tregs by CD11c$^+$ cells. The CD11c$^+$ cells were isolated from treated tumors and seeded in a 48-well plate (1×10^5 cells per well), and after incubation for 24 h (n=4) (left panel), IL-6 production from the CD11c$^+$ cells was measured by ELISA. Target cells (CD4$^+$CD25$^-$ T cell) and Treg (CD4$^+$CD25$^+$ T cell) were isolated from the spleen of naïve BALB/c mice, and were co-cultured with the designated CD11c$^+$ cells in a CD3-coated 96-well plate, and the proliferation of target cells was examined by ^{3}H-thymidine uptake assay (n=3) (right panel). The experiments were repeated three times. (**c**) IL-6-mediated suppression of Treg activity. Target cells and Tregs were cultured in a CD3-coated 96-well plate with the supernatant of CD11c$^+$cells from treated tumors, and the proliferation of target cells was evaluated by ^{3}H-thymidine uptake assay (n=3). The addition of anti-IL-6 antibody (R&D systems) was used to neutralize mouse IL-6 in the medium. The experiments were repeated twice. (**d**) The frequency of Tregs in the spleen and treated tumors. The lymphocytes were collected from the spleens (n=4, left panel) and treated tumor (n=3, right panel), and Foxp3$^+$ and CD4$^+$ cells were analyzed by flow cytometry.

flushing each femur and tibia with RPMI-1640 medium (RPMI) supplemented with 5% heat-inactivated fetal bovine serum (ICN Biomedicals, Inc., Irvine, CA, USA), and splenic cells were prepared by macerating the spleens. After lysis of the erythrocytes, splenic cells were incubated with anti-Thy-1.2 immunomagnetic beads (Miltenyi Biotec GmbH, Bergisch Gladbach, Germany) at 4 °C for 15 min, followed by selection of T cells by AutoMACS (Miltenyi Biotec).

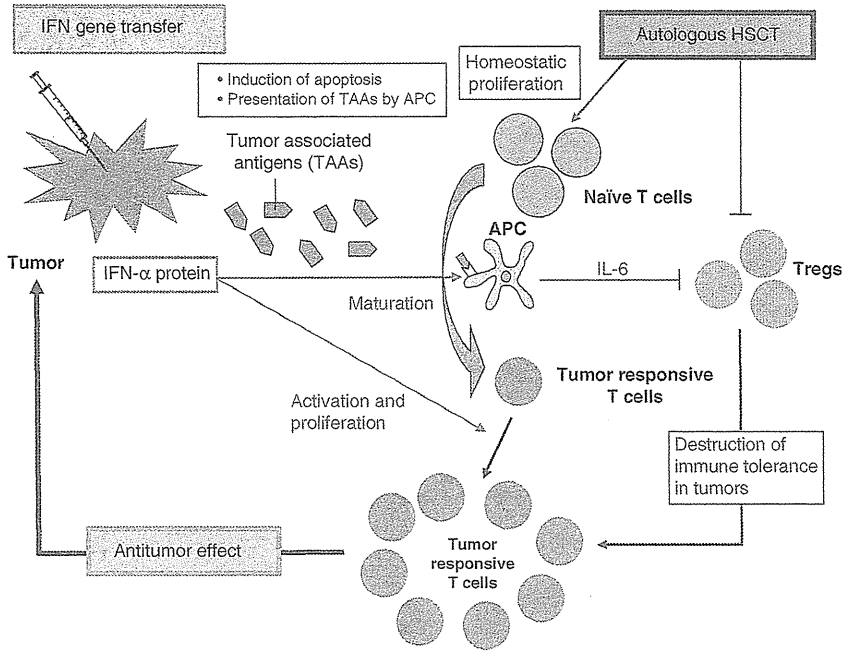

Figure 8 Model showing integrated mechanisms of inducing strong tumor immunity by a combination therapy. In the 'homeostatic proliferation' condition after synHSCT, T cells effectively recognize the low-affinity self-antigen including TAAs, leading to an induction of antitumor immunity. The conditioning of HSCT with irradiation and/or immunosuppressive reagents can destroy the immunotolerance mechanisms developed by the tumor. Furthermore, IFN-α expression in the tumors exposes TAAs in large quantity to DCs, and IFN-α promotes maturation and enhances the antigen-presenting capacity of DCs. In addition, DCs produced a significant amount of IL-6 in response to IFN-α, which suppress the proliferation and activity of Tregs. The integrated mechanisms are capable of inducing a strong antitumor immunity against solid cancers.

Tumor cell lines, recombinant adenovirus vectors and plasmid vectors

CT26 and Renca (American Type Culture Collection, Rockville, MD, USA) are weakly immunogenic BALB/c-derived colon and renal cancer cell lines, respectively. Cells were maintained in RPMI containing 10% fetal bovine serum, 2 mM L-glutamine and 0.15% sodium bicarbonate (complete RPMI). A CT26 cell line that stably expresses the firefly luciferase gene was generated by retrovirus vector-mediated transduction and designated as CT26-Luc. The recombinant adenovirus vectors expressing mouse interferon-α (Ad-mIFN) and alkaline phosphatase cDNA (Ad-AP) were prepared as described.[23,24] The recombinant adenoviruses are based on serotype 5 with deletions of the entire E1 and a part of the E3 regions, and have the CAG promoter, which is a hybrid of the cytomegalovirus immediate early enhancer sequence and the chicken β-actin/rabbit β-globin promoter. A cesium chloride-purified virus was desalted using a sterile Bio-Gel P-6 DG chromatography column (Econopac DG 10; Bio-Rad, Hercules, CA, USA) and diluted for storage in a 13% glycerol/phosphate-buffered saline solution. All viral preparations were confirmed by PCR assay to be free of $E1^+$ adenovirus. A plasmid DNA (pIFN-α) expressing the *IFN-α* gene under the control of the CAG promoter was also used for intratumoral gene transfer. The plasmids that express an alkaline phosphatase (pAP) or luciferase gene (pLuc) were used as a negative control.

In vitro cell proliferation assay

Cultured cells were seeded at 2×10^3 per well in 96-well plates and plasmid DNA-liposome (Lipofectamine2000; Invitrogen, Carlsbad, CA, USA) complex was added according to the manufacturer's protocol. The cell numbers were assessed by a colorimetric cell viability assay using a water-soluble tetrazolium salt (Tetracolor One; Seikagaku Corp., Tokyo, Japan) at 5 days after the transfection. Absorbance was determined by spectrophotometry using a wavelength of 450 nm with 595 nm as a reference. The assays (carried out in four wells) were repeated three times.

In vivo tumor inoculation and *IFN-α* gene transfer

CT26 cells (1×10^6) or Renca cells (5×10^6) were injected subcutaneously into the leg of BALB/c mice. When the subcutaneous tumor was established (~0.6 cm in diameter), it was injected once with 50 μl of Ad-mIFN or control vector (Ad-AP). Plasmid DNA–liposome complex was prepared by the addition of 30 μg plasmid DNA into a total of 75 μl phosphate-buffered saline per mouse, followed by the addition of 75 μl of 0.15 mmol l^{-1} DMRIE-DOPE ((+/–)-*N*-(2-hydroxyethyl)-*N*, *N*-dimethyl –2,3-bis(tetradecyloxy)-1-propanaminium bromide/dioleoylphosphatidylethanolamine), which was provided from Vical, Inc., (San Diego, CA, USA). The mixture solution was incubated at room temperature for 15 min, and then injected directly into the tumor three times every other day. The shortest (r) and longest (l) tumor diameters were measured at indicated days and the tumor volume was determined as $r^2l/2$. Data are presented as mean ± s.d. The experiments were repeated two times.

Enzyme-linked immunosorbent spot assays

IFN-γ ELISpot kit (BD Bioscience, San Jose, CA, USA) was used according to the manufacturer's instructions. Briefly, splenocytes (1×10^5) and mitomycin C-treated tumor cells (1×10^4) were co-cultured in 96-well plates pre-coated with mouse IFN-γ (BD Bioscience) for 20 h at 37 °C in complete RPMI medium in triplicate. After washing the wells, biotinylated anti-mouse IFN-γ antibody (2 μg ml^{-1}) was added and incubated for 2 h at room temperature. Then, a streptavidin-horseradish peroxidase solution was added and incubated for 1 h at room temperature. After the addition of an aminoethyl carbozole substrate solution, spots were counted under a stereomicroscope.

Flow cytometry of cell surface marker and intracellular cytokine staining

Allo-phycocyanin-conjugated monoclonal antibody (mAb) to identify mouse IFN-γ and fluorescein isothiocyanate-conjugated mAb to detect CD4, CD8 and CD49b were purchased from BD Pharmingen (San Jose, CA, USA). Splenocytes (1×10^6) were incubated with medium alone (control) or CT26 (1×10^5) cells

for 2 days; brefeldin-A (10 μg ml^{-1}) was then added for 2 h of incubation. After washing, cells were incubated with the CD4, CD8 or CD49b mAbs in a total volume of 100 μl phosphate-buffered saline with 5% fetal bovine serum for 30 min at 4 °C, and then fixed and permeabilized with a permeabilization buffer (BD Biosciences). Cells were finally stained with antibody to IFN-γ for 15 min at room temperature, washed again and analyzed by FACSCalibur (BD Biosciences). Irrelevant immunoglobulin G mAbs were used as a negative control. Ten thousand live events were acquired for analysis.

Cytotoxic assays

An *in vitro* cytotoxic assay was performed as previously described.[12] Briefly, splenocytes were cultured for 4 days with mitomycin C-treated CT26 stimulators, and then the responder cells were collected and used as effector cells. CT26 target cells were labeled with ^{51}Cr (Perkin-Elmer Japan Co., Kanagawa, Japan). For a 4 h chromium release assay, 4×10^5, 1×10^5 and 5×10^4 effector cells were mixed with 1×10^4 target cells in a 96-well round-bottom plate (Corning Incorporated, New York, NY, USA). To evaluate the relative contributions of CD4$^+$ and CD8$^+$ T cells for the tumor cell lysis, effector cells were incubated with mAbs against mouse CD4 (L3L4; BD Pharmingen) or CD8 (Ly-2; BD Pharmingen) for 1 h at 37 °C before mixing with target cells. Supernatants were harvested and counted in a gamma counter (Packard Bioscience Company, Meriden, CT, USA). The percentage of cytotoxicity was calculated as ((experimental c.p.m.–spontaneous c.p.m.)/(maximum c.p.m.–spontaneous c.p.m.))×100. Each assay was carried out in triplicate.

Immunohistochemistry

Immunostaining was performed using streptavidin-biotin-peroxidase complex techniques (Nichirei, Tokyo, Japan). Consecutive cryostat tissue sections (6 μm) were mounted on glass slides and fixed in 99.5% ethanol for 20 min. After blocking with normal rat serum, the sections were stained with rat anti-mouse CD4 and CD8 antibodies (BD Pharmingen). Parallel negative controls with antibodies of the same isotype were examined in all cases. The sections were counter-stained with methyl green.

In vivo depletion of T and NK cells

To deplete the subsets of immune effector cells before and during the treatment with *IFN-α* gene transfer, the synHSCT mice received intraperitoneal injections of 0.3 mg. Monoclonal antibody from the anti-CD4$^+$ hybridoma (clone GK1.5, rat IgG2b) or 1.5 mg mAb from the anti-CD8$^+$ hybridoma (clone Lyt–2.1, mouse IgG2b; see Nakayama and Uenaka[25]) or 0.5 mg of anti-asialo GM1 antibody (targeting NK cells: Wako Pure Chemical Industries, Ltd, Tokyo, Japan). Administration of antibodies started at 2 days after the inoculation of CT26 cells, and the injection was repeated every 5–6 days, throughout the entire experimental period. Flow cytometry showed that ~80% of CD4$^+$, ~60% of CD8$^+$ T cells and ~80% of NK cells were depleted in the Ab-treated mice.

In vivo imaging of the tumors in a liver-metastasis model

CT26-Luc cells were injected beneath the splenic capsule to generate liver metastasis. The BALB/c mice with CT26-Luc tumors were administered with D-luciferin (150 mg kg^{-1}) (Wako Pure Chemical Industries) by intraperitoneal injection. At 10 min later, photons from animal whole bodies were counted using an *in vivo* imaging system.

Isolation of CD11c+ cells and T-cell proliferation assay

Dendritic cells were isolated using mouse CD11c MicroBeads and AutoMACS magnetic sorter (Miltenyi Biotec) from tumors of non-HSCT mice treated by intratumoral *IFN-α* gene transfer, tumors of synHSCT mice injected with control plasmid and tumors of synHSCT mice treated by intratumoral *IFN-α* gene transfer, and designated as IFN-CD11c$^+$, HSCT-CD11c$^+$ and IFN/HSCT-CD11c$^+$, respectively. The flow cytometry showed that ~90% of isolated cells express CD11c, and that ~80% of the isolated CD11c$^+$ cells are negative for CD14 (macrophage marker), suggesting that a major population of isolated CD11c$^+$ cells is DCs. CD4$^+$CD25$^+$ or CD4$^+$CD25$^-$ T cells were isolated from the spleen of naïve BALB/c mice using mouse CD4 pre-enrichment kit, mouse CD25 selection kit and RoboSep magnetic sorter (StemCell Technologies, Vancouver, BC, Canada). These populations were stained with anti-Foxp3 antibody, and flow cytometry revealed that about 80% of CD4$^+$CD25$^+$cells expressed Foxp3. CD4$^+$CD25$^-$ T cells were incubated in a 96-well plate (1×10^4 per well) with 2×10^3 of CD11c$^+$ cells, 0.5 μg ml^{-1} of anti-CD3 antibody and the indicated number of CD4$^+$CD25$^+$ T cells for 48 h. T-cell proliferation was determined as ^{3}H-thymidine incorporation during the last 12 h of culture.

Statistical analysis

Comparative analyses of the data were performed by the Student's *t*-test, using SPSS statistical software (SPSS Japan Inc., Tokyo, Japan). $P<0.05$ was considered as a significant difference.

CONFLICT OF INTEREST

The authors declare no conflict of interest.

ACKNOWLEDGEMENTS

This work was supported in part by a grant-in-aid for the 3rd Term Comprehensive 10-year Strategy for Cancer Control from the Ministry of Health, Labour and Welfare of Japan, by grants-in-aid for Cancer Research from the Ministry of Health, Labour and Welfare of Japan and by the program for promotion of Foundation Studies in Health Science of the National Institute of Biomedical Innovation (NIBIO) and by Kobayashi Foundation for Cancer Research. H Hara and T Udagawa are awardees of a Research Resident Fellowship from the Foundation for Promotion of Cancer Research. We thank Vical Incorporated for providing the DMRIE/DOPE liposome.

1 Rabinovich GA, Gabrilovich D, Sotomayor EM. Immunosuppressive strategies that are mediated by tumor cells. *Annu Rev Immunol* 2007; **25**: 267–296.
2 Wrzesinski C, Restifo NP. Less is more: lymphodepletion followed by hematopoietic stem cell transplant augments adoptive T-cell-based anti-tumor immunotherapy. *Curr Opin Immunol* 2005; **17**: 195–201.
3 Hu HM, Poehlein CH, Urba WJ, Fox BA. Development of antitumor immune responses in reconstituted lymphopenic hosts. *Cancer Res* 2002; **62**: 3914–9391.
4 Dummer W, Niethammer AG, Bacccala R, Lawson BR, Wagner N, Reisfeld RA *et al.* T cell homeostatic proliferation elicits effective antitumor autoimmunity. *J Clin Invest* 2002; **110**: 185–192.
5 Borrello I, Sotomayor EM, Rattis FM, Cooke SK, Gu L, Levitsky HI. Sustaining the graft-versus-tumor effect through posttransplant immunization with granulocyte-macrophage colony-stimulating factor (GM-CSF)-producing tumor vaccines. *Blood* 2000; **95**: 3011–3019.
6 Kobayashi A, Hara H, Ohashi M, Nishimoto T, Yoshida K, Ohkohchi N *et al.* Allogeneic MHC gene transfer enhances an effective antitumor immunity in the early period of autologous hematopoietic stem cell transplantation. *Clin Cancer Res* 2007; **13**: 7469–7479.
7 Pfeffer LM, Dinarello CA, Herberman RB, Williams BR, Borden EC, Bordens R *et al.* Biological properties of recombinant α-Interferons: 40th anniversary of the discovery of interferons. *Cancer Res* 1998; **58**: 2489–2499.
8 Belardelli F, Ferrantini M, Proietti E, Kirkwood JM. Interferon-alpha in tumor immunity and immunotherapy. *Cytokine Growth Factor Rev* 2002; **13**: 119–134.
9 Santini SM, Lapenta C, Santodonato L, D'Agostino G, Belardelli F, Ferrantini M. IFN-alpha in the generation of dendritic cells for cancer immunotherapy. *Handb Exp Pharmacol* 2009; **188**: 295–317.
10 Ferrantini M, Capone I, Belardelli F. Dendritic cells and cytokines in immune rejection of cancer. *Cytokine Growth Factor Rev* 2008; **19**: 93–107.
11 Hara H, Kobayashi A, Yoshida K, Ohashi M, Ohnami S, Uchida E *et al.* Local interferon-α gene therapy elicits systemic immunity in a syngeneic pancreatic cancer model in hamster. *Cancer Sci* 2007; **98**: 455–463.
12 Hara H, Kobayashi A, Narumi K, Kondoh A, Yoshida K, Nishimoto T *et al.* Intratumoral interferon-α gene transfer enhances tumor immunity after allogeneic hematopoietic stem cell transplantation. *Cancer Immunol Immunother* 2009; **58**: 1007–1021.
13 Narumi K, Kondoh A, Udagawa T, Hara H, Goto N, Ikarashi Y *et al.* Administration route-dependent induction of antitumor immunity by interferon-alpha gene transfer. *Cancer Sci* 2010; **101**: 1686–1694.
14 Rodriguez EG. Nonviral DNA vectors for immunization and therapy: design and methods for their obtention. *J Mol Med* 2004; **82**: 500–509.
15 Ohtani H. Focus on TILs: prognostic significance of tumor infiltrating lymphocytes in human colorectal cancer. *Cancer Immunity* 2007; **7**: 4–13.
16 Garcia CA, Wang H, Benakanakere MR, Barrett E, Kinane DF, Martin M. c-Jun controls the ability of IL-12 to induce IL-10 production from human memory CD4$^+$ T cells. *J Immunol* 2009; **183**: 4475–4482.
17 Pasare C, Medzhitov R. Toll pathway-dependent blockade of CD4$^+$CD25$^+$ T-cell-mediated suppression by dendritic cells. *Science* 2003; **299**: 1033–1036.

18 Curiel TJ, Coukos G, Zou L, Alvarez X, Cheng P, Mottram P *et al.* Specific recruitment of regulatory T cells in ovarian carcinoma fosters immune privilege and predicts reduced survival. *Nat Med* 2004; **10**: 942–949.
19 Lai G, Zhang N, van der Touw W, Ding Y, Ju W, Bottinger EP *et al.* Epigenetic regulation of Foxp3 expression in regulatory T cells by DNA methylation. *J Immunol* 2009; **182**: 259–273.
20 Grivennikov S, Karin E, Terzic J, Mucida D, Yu GY, Vallabhapurapu S *et al.* IL-6 and Stat3 are required for survival of intestinal epithelial cells and development of colitis-associated cancer. *Cancer Cell* 2009; **15**: 103–113.
21 Asavaroengchai W, Kotera Y, Mule JJ. Tumor lysate-pulsed dendritic cells can elicit an effective antitumor immune response during early lymphoid recovery. *Proc Natl Acad Sci USA* 2002; **99**: 931–936.
22 Morgan RA, Dudley ME, Wunderlich JR, Hughes MS, Yang JC, Sherry RM *et al.* Cancer regression in patients after transfer of genetically engineered lymphocytes. *Science* 2006; **314**: 126–129.
23 Aoki K, Barker C, Danthinne X, Imperiale MJ, Nabel GJ. Efficient generation of recombinant adenoviral vectors by Cre-lox recombination *in vitro*. *Mol Med* 1999; **5**: 224–231.
24 Ohashi M, Yoshida K, Kushida M, Miura Y, Ohnami S, Ikarashi Y *et al.* Adenovirus-mediated interferon α gene transfer induces regional direct cytotoxicity and possible systemic immunity against pancreatic cancer. *Br J Cancer* 2005; **93**: 441–449.
25 Nakayama E, Uenaka A. Effect of *in vivo* administration of Lyt antibodies. *J Exp Med* 1985; **161**: 345–355.

SCIENTIFIC REPORTS

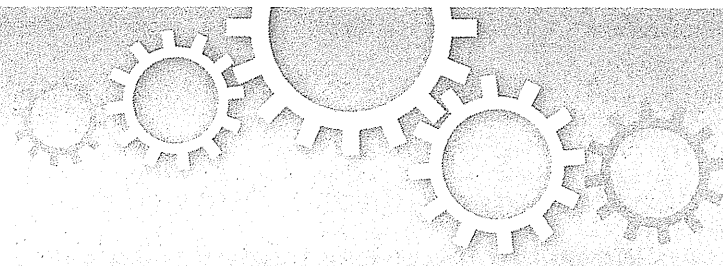

SUBJECT AREAS:
PLURIPOTENCY
EMBRYONIC STEM CELLS
CANCER MODELS
MECHANISMS OF DISEASE

Received
17 July 2012

Accepted
29 October 2012

Published
10 December 2012

Correspondence and requests for materials should be addressed to T.O. (tochiya@ncc.go.jp)

Two distinct knockout approaches highlight a critical role for p53 in rat development

Masaki Kawamata & Takahiro Ochiya

Division of Molecular and Cellular Medicine, National Cancer Center Research Institute, 1-1, Tsukiji, 5-chome, Chuo-ku, Tokyo 104-0045, Japan.

Gene targeting in embryonic stem cells (ESCs) has become the principal technology for generating knockout models. Although numerous studies have predicted that the disruption of *p53* leads to increased developmental anomalies and malignancies, most *p53* knockout mice develop normally. Therefore, the role of *p53* in animal development was examined using rat knockout models. Conventionally generated homozygous KO males developed normally, whereas females rarely survived due to neural tube defects. Mutant chimeras generated via blastocyst injection with *p53*-null ESCs exhibited high rates of embryonic lethality in both sexes. This phenotype could be observed in one month by the use of zinc-finger nucleases. The *p53*-null ESCs were resistant to apoptosis and differentiation, and exhibited severe chromosome instabilities in the chimera-contributed cells, suggesting an essential role for p53 in maintaining ESC quality and genomic integrity. These results demonstrate that p53 functions as a guardian of embryogenesis in the rats.

Over the past two decades, knockout (KO) technology in mice has helped to clarify the physiological function of a large number of genes. However, unexpected phenotypes have been observed in some cases, making it difficult to understand the role of the deleted gene, or to translate that data to the phenotypes of human diseases caused by mutations in such genes. Thus, gene-targeting techniques for other animals, such as rats, have long been sought. Many strategies for manipulating rat genes to generate loss-of-function models have been adapted from the mouse genetic toolbox, including conventional transgenesis by pronuclear injection[1], RNA interference[2], N-ethyl-N-nitrosourea (ENU) mutagenesis[3,4], and transposon mutagenesis[5–7]. KO rats have been produced using Zinc-finger nuclease (ZFN) technology[8,9], and, most recently, germline-competent rat ESCs and rat induced pluripotent stem cells (iPSCs) have been established by the addition of cell-signaling inhibitors to the culture medium[10–13], making it possible to generate both transgenic (Tg)[12,14] and KO rats[15].

The tumor suppressor gene *p53* is a good example of a gene whose function in mouse development requires further scrutiny. Donehower et al. first reported normal Mendelian ratios and postnatal development in *p53* homozygous KO mice[16]. However, two other groups later showed that a fraction of homozygous KO females had fatal embryonic exencephaly, a defect in neural tube closure that results in an overgrowth of neural tissue in the midbrain region[17,18]. Such results indicate that, at least in some cases, p53 influences development in females[19]. In the case of *p53* homozygous KO rats, neural tube defects (NTDs) in females were not found but increased susceptibility to tumor development was reported[15,20,21].

p53 has been shown to regulate not only cell cycle arrest, apoptosis, and DNA repair in many types of cells[22], but also stemness, by suppressing *Nanog* expression in ESCs[23]. Considering these observations, malignant transformations may occur in *p53*-null ESCs and chimera development may be hindered. However, chimeric mutant mice have been successfully generated via the injection of blastocysts with iPSCs derived from *p53*-null mouse embryonic fibroblasts (MEFs), and germline transmission of the *p53*-null cells was also accomplished[24,25]. The properties of rat ESCs differ from those of mouse ESCs in that rat ESCs cannot be cultured in mouse ESC culture conditions due to their high sensitivity to differentiation signals[26]. Thus, an approach using *p53*-null rat ESCs might reveal new insights into the function of p53 in regulating stemness and animal development.

We previously generated *Oct4*-Venus Tg rats, and established *Oct4*-Venus ESC lines in which *Oct4* expression can be monitored by green fluorescence[12,27]. Here, both conventionally KO and mutant chimeras rats were generated using *p53*-null *Oct4*-Venus ESCs, and their development was investigated. Moreover, an efficient

method for a rapid generation of mutant chimeras was developed using ZFN-mediated gene targeting in rat ESCs. Using this method, developmental phenotypes can be observed within 1 month.

Results

Conventionally generated $p53^{-/-}$ females reveal the cause of NTDs. *p53* homozygous KO rats were generated via germline transmission of heterozygous $p53^{+/C}$ ESCs (Fig. 1a,b,e). The details are described in the *Materials and Methods*. The Mendelian ratios in weaned rats produced from heterozygous intercrosses were investigated (Fig. 2a). The frequency of homozygous $p53^{C/C}$ rats was 16.9%, less than the anticipated value of 25% (Table 1). Moreover, only one $p53^{C/C}$ female developed normally, frequency = 0.70%, significantly less than 16.2% $p53^{C/C}$ males. These results suggest that most of the $p53^{C/C}$ females either do not survive gestation, or die after birth but prior to weaning. To investigate the developmental dysfunctions in $p53^{C/C}$ females, litters from heterozygous intercrosses were examined at embryonic day 16.0 (E16.0) to E18.0. Eleven $p53^{C/C}$ female embryos (12.8%, 11/86) were recovered at this stage; six (57%, 6/11) exhibited exencephaly (Table 1) and two of these also exhibited spina bifida (Fig. 2b). Although these two abnormalities are the most prevalent NTDs, spina bifida in *p53* mutant mice has only been reported in one study[28]. Exencephaly was only found in the female embryos, consistent with previous observations of a higher incidence of NTDs in human females and in numerous mouse models[29]. Expression of SOX2, a marker for primordial neuronal cells

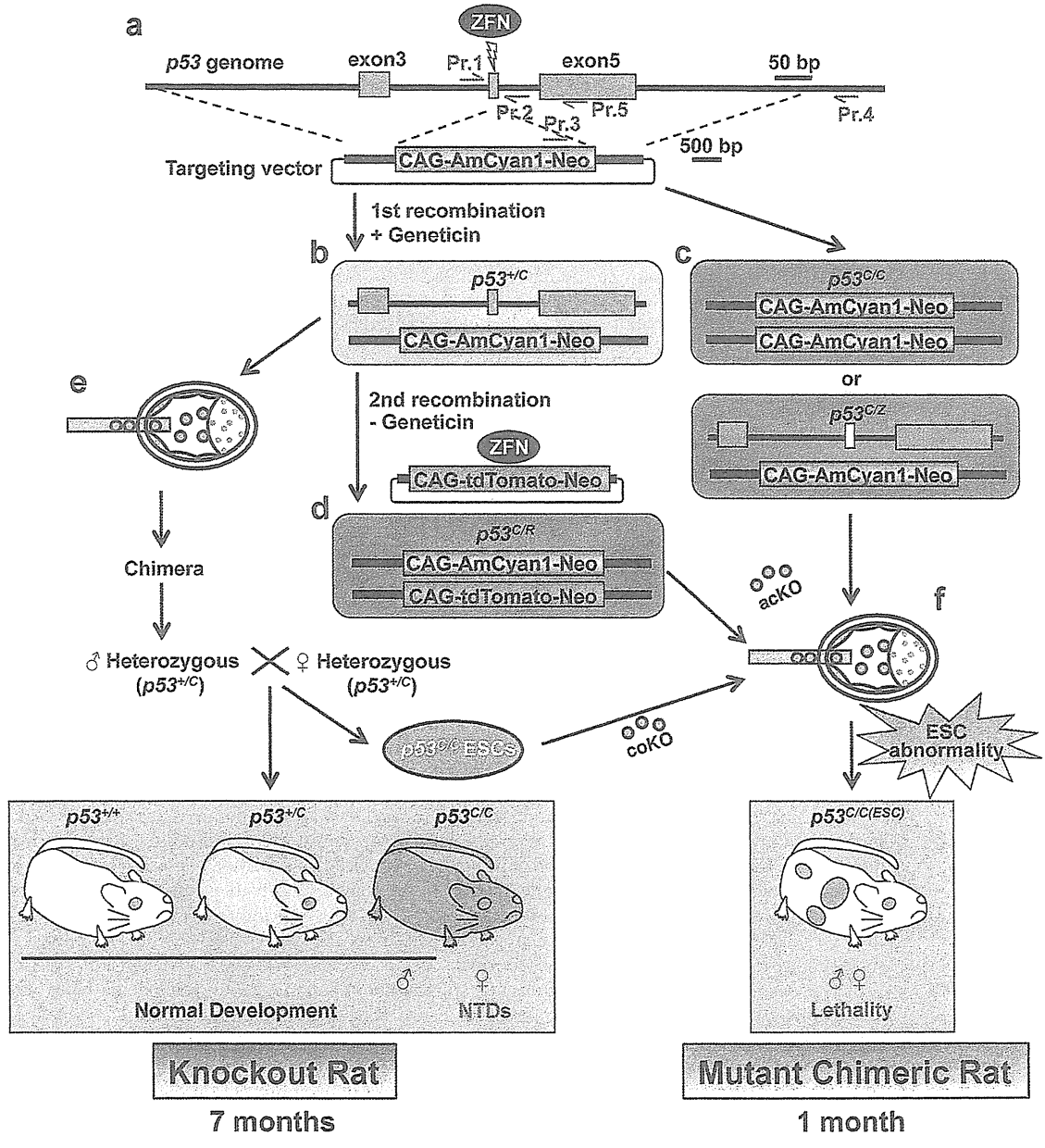

Figure 1 | Schematic representation of *p53* KO strategy in rats. (a–d) Both mono- (b) and bi-allelic (c) or 2ndary (d) homologous recombination are induced by ZFN. (e, f) Heterozygous or homozygous ESC-injection leads to the generation of conventionally generated KO model (e) or ESC-based mutant chimeric models (f), respectively. A yellow box indicates a frame shift mutation induced by ZFNs. Pr., Primer. coKO, congenital KO. acKO, acquired KO.

Table 1 | The *p53* Genotypes of Adult and Embryonic Rats

Genotype	$p53^{+/+}$	$p53^{+/C}$	$p53^{C/C}$	$p53^{C/C}$ Exencephaly
Adults	41 (28.9%)	77 (54.2%)	24 (16.9%)	0
Male	18 (12.7%)	42 (29.6%)	23 (16.2%)	0
Female	23 (16.2%)	35 (24.6%)	1 (0.70%)	0
Embryos	21 (24.4%)	48 (55.8%)	17 (19.8%)	6
Male	11 (12.8%)	22 (25.6%)	6 (7.0%)	0
Female	10 (11.6%)	26 (30.2%)	11 (12.8%)	6 (54.5%)[a]

[a]Of the 11 $p53^{C/C}$ female embryos, six exhibited exencephaly.

expressed in the embryonic neural plate[30], was detected on the surface of the brain and in areas of spina bifida (Fig. 2d, arrowheads), confirming that neural tube closure had failed. Compared to a $p53^{+/C}$ embryo (Fig. 2e, right), the aberrant ventricular zone (VZ) structure in the brain of a $p53^{C/C}$ exencephalic embryo was revealed by the localization of SOX2 (Fig. 2d left, arrows), which is expressed in the neuroendothelial stem cells of the VZ[31]. In this embryo, *Oct4*-Venus expressing cells were aberrantly located in the exencephalic region (Fig. 2b, green square, and 2c).

Embryonic lethality in a mutant chimeric model. ZFNs can create site-specific double-strand breaks, which are repaired via non-homologous end joining, resulting in frame-shift mutations by the arbitrary addition or deletion of base pairs. Cotransfection of ZFNs with targeting vectors enhances homologous recombination, not only in human pluripotent cells[32,33], but also in one-cell embryos, leading to the direct generation of knock-in mice[34] and rats[35]. In the present work, ZFNs were used to produce homozygous mutant ESC lines by a single recombination step (Fig. 1c). Using this approach, 1 of 46 (2.2%) clones harbored dual knock-in alleles ($p53^{C/C}$), while 7 of 46 (15%) clones possessed both knock-in and frame shift mutant alleles ($p53^{C/Z}$). In a 2nd-step recombination, homozygous clones were also produced from a $p53^{+/C3}$ ESC clone based on the same strategy using both ZFNs and a targeting vector expressing red fluorescence (Fig. 1b,d). A successful homologous recombination was achieved in 3 of 8 clones (38%, $p53^{C/R}$; Supplementary Fig. S2c). These ESC lines were called acquired KO (acKO) ESCs (Fig. 1c). The contribution of $p53^{-/-}$ ($p53^{C/C}$, $p53^{C/Z}$, or $p53^{C/R}$) ESCs to rats, which are called $p53^{-/-\,(ESC)}$ rats, was examined, and the timeline for the rapid generation of the mutant chimeras is shown schematically (Fig. 3a,b). Microinjection of $p53^{-/-}$ ESCs into blastocysts led to the delivery of only a few pups (0.4 ± 0.2 per foster mother, n=5, 4 cell lines). This number (0.4 ± 0.2/foster mother) was significantly smaller than the number of pups delivered following injection of $p53^{+/+}$ ESCs into blastocysts (4.0 ± 1.1 per foster mother, n=5, 3 cell lines, $P<0.05$) or $p53^{+/-}$ ($p53^{+/C}$) ESCs (5.1 ± 1.1 per foster mother, n=9, 4 cell lines, $P<0.05$) (Fig. 3c). The

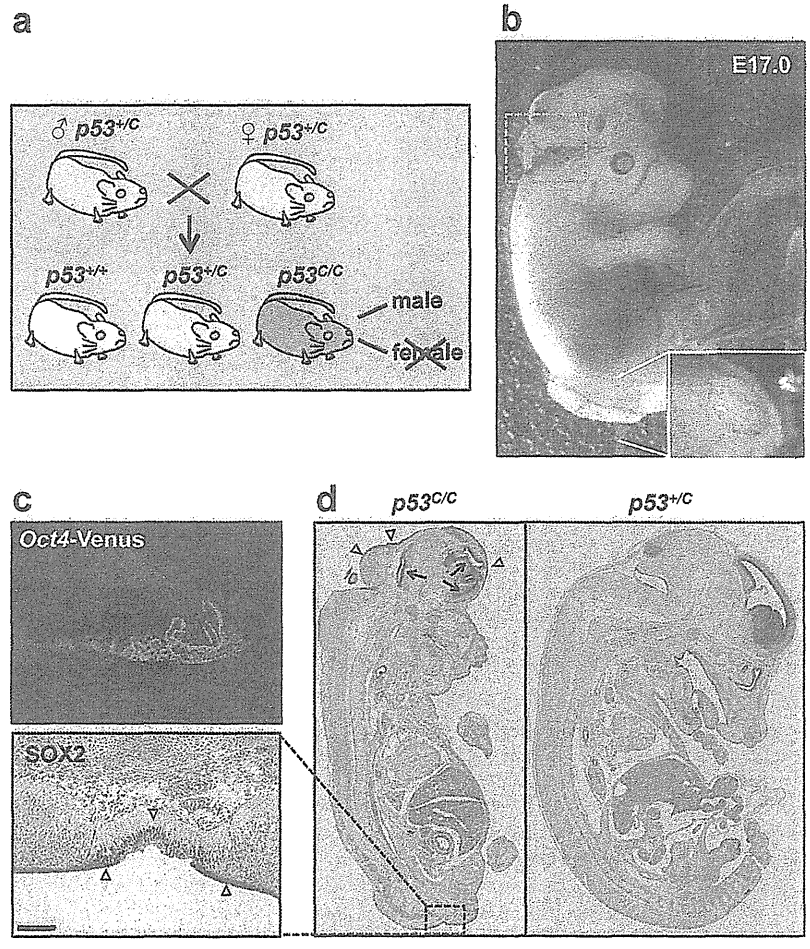

Figure 2 | Phenotypes in conventionally generated p53 homozygous rats. (a) Schematic representation of heterozygous intercrosses indicates a loss of adult female. (b) An embryo at day 17.0 of gestation (E17.0) displaying exencephaly and spina bifida. A dotted green square indicates (c). (c) Fluorescence image of the area inside the dotted green square in (b). *Oct4*-Venus fluorescence is observed in the exencephalic region. (d) IHC staining for SOX2 identifies positive cells in the ventricular zone (arrows) and surface (arrowheads) of both brain and spina bifida (magnified image, scale bar = 100 μm).

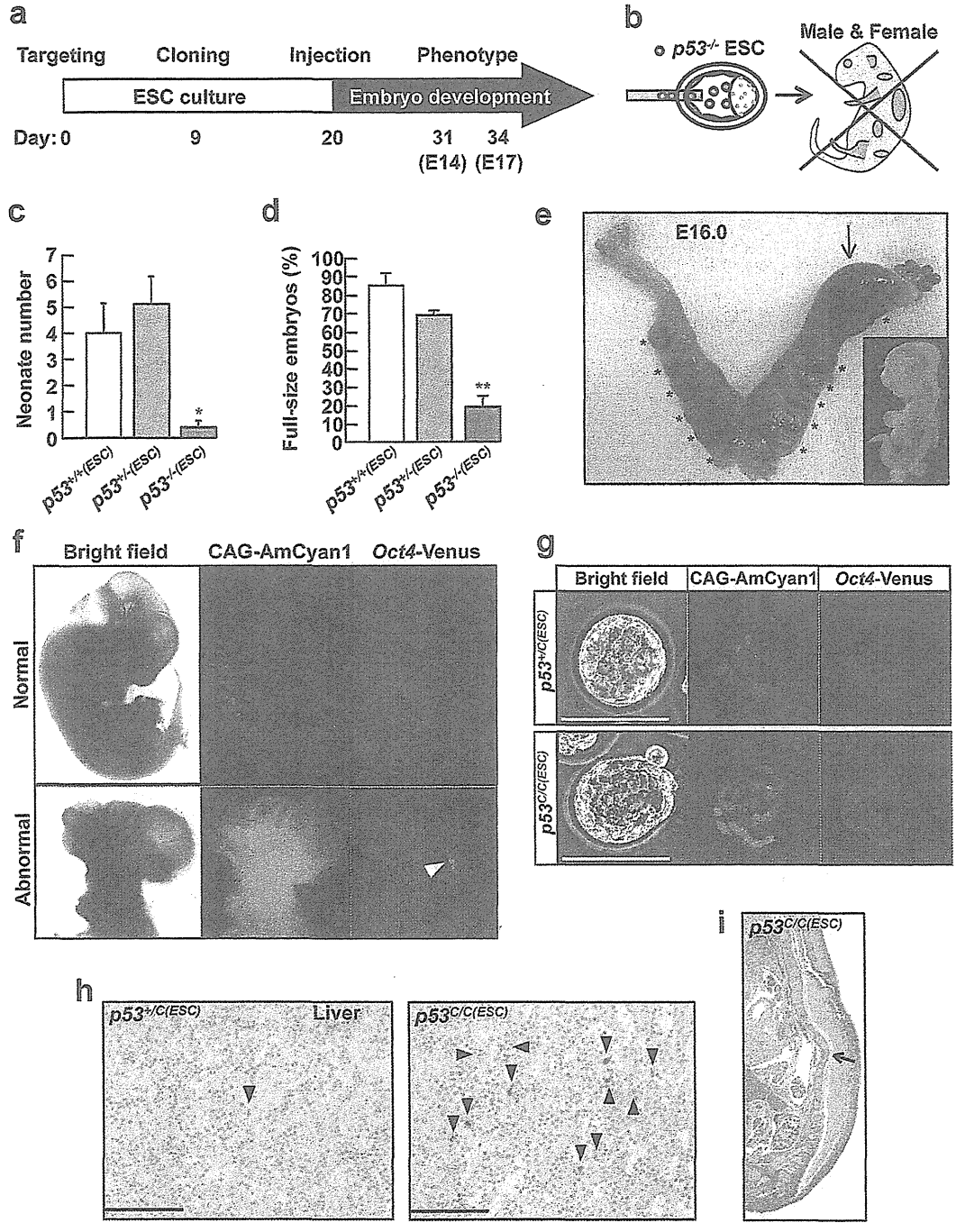

Figure 3 | Embryonic lethality in p53 mutant chimeras. (a) Time line for generating $p53^{-/-\,(ESC)}$ chimeras and (b) Schematic representation to investigate phenotype during embryogenesis. (c) Number of neonates successfully delivered. $p53^{+/+}$ (n=5, 3 cell lines), $p53^{+/-}$ (n=9, 4 cell lines) or $p53^{-/-}$ (n=5, 4 cell lines) ESCs were injected into wild-type blastocysts. n, injection number. *, $P<0.05$, $p53^{-/-}$ vs. $p53^{+/+}$ and $p53^{+/-}$. (d) The ratio of chimeric embryos with normal body size at E14.0 to E17.0. $p53^{+/+}$ (n=4, 4 cell lines), $p53^{+/-}$ (n=7, 4 cell lines) or $p53^{-/-}$ (n=14, five cell lines) ESCs were injected into wild-type blastocysts. n, injection number. **, $P<0.001$, $p53^{-/-}$ vs. $p53^{+/+}$ and $p53^{+/-}$. (e) Developmental dysfunction in chimeric embryos injected with $p53^{C/R2}$ ESCs at E16.0. An arrow indicates a chimera with growth retardation (inset). Asterisks indicate fetal absorption. (f) Correlation between developmental dysfunction and ESC contribution. $p53^{C/C1}$ ESCs expressing AmCyan1 contribute to chimeric embryos at E14.0. An arrowhead indicates an ectopic expression of *Oct4*-Venus. (g) $p53^{C/R4}$ ESC proliferation in blastocyst. Twelve ESCs were injected into blastocyst, followed by incubation overnight in YPAC medium. (h) Immunohistochemistry using Cleaved-Caspase3 antibody in liver of $p53^{+/C(ESC)}$ or $p53^{C/C(ESC)}$ chimera. Arrowheads indicate the apoptotic cells. (i) Spinal curvature (an arrow) in $p53^{C/C(ESC)}$ chimera. All scale bars = 100 μm.

newborns derived from $p53^{-/-}$ ESC-injections did not exhibit a brown coat-color, indicating that they were not chimeras. Because these results suggest that the development of $p53^{-/-\,(ESC)}$ embryos was defective, fetal development at stages E14.0 to E17.0 was examined. Approximately 80% of the $p53^{-/-\,(ESC)}$ embryos (n=14, 5 cell lines, Fig. 3d) showed abnormal development resulting in complete

resorption (Fig. 3e, asterisks) or growth retardation (Fig. 3e, an arrow and inset). A large number of $p53^{-/-}$ ESC-derived cells were detected in these embryos (Fig. 3f, lower). However, the remaining $p53^{-/-(ESC)}$ embryos (30/189 embryos: 20.0 ± 5.6%) developed a normal body size (Fig. 3f, upper and Supplementary Table S1). The number of normal embryos (20.0 ± 5.6%) was significantly lower than that of $p53^{+/+(ESC)}$ embryos (53/63 embryos: 85.1 ± 5.8%, n=4, 4 cell lines, $P<0.01$) or $p53^{+/-(ESC)}$ embryos (44/64 embryos: 69.0 ± 2.2%, n=7, 4 cell lines, $P<0.01$) (Fig. 3d). Among the normal-sized $p53^{-/-(ESC)}$ embryos, 26 of 30 (87.8 ± 9.7%, n=10, 5 cell lines) embryos were chimeras, whereas 22 of 26 displayed a relatively lower contribution of the mutant cells. Although the number of $p53^{+/-(ESC)}$ chimera (30/44 embryos, 66.9 ± 6.6%, n=7, 4 cell lines) was similar to that of $p53^{-/-(ESC)}$ chimera ($P=0.14$), the $p53^{+/-(ESC)}$ chimeras developed normally (Fig. 3c, d). The number of $p53^{+/+(ESC)}$ chimera (17/53 embryos, 36.0 ± 10.2%, n=4, 4 cell lines) was significantly smaller than that of either $p53^{+/-(ESC)}$ ($P=0.044$) or $p53^{-/-(ESC)}$ ($P=0.0081$) chimera. These results suggest that *p53* mutation enhances the chimeric contribution of ESCs and the high contribution of *p53*-null ESCs induces embryonic lethality.

To address the mechanisms by which $p53^{-/-}$ ESCs result in embryonic lethality, the behavior of $p53^{-/-}$ ESCs was followed in blastocysts incubated *in vitro*. Blastocysts were injected with 12 ESCs and incubated over night. Although $p53^{+/+1}$ ESCs remained in the blastocysts, the number decreased to 4.0 ± 0.89 cells (Fig. 3g, upper, n=5). In contrast, a significantly larger number of $p53^{C/R4}$ ESCs (13.7 ± 1.2 cells, n=7, $P<0.0001$) were detected (Fig. 3g, lower), indicating proliferation of the *p53*-null ESCs in the blastocysts. The excess proliferation may lead to a high ESC contribution, resulting in the developmental abnormalities that led to resorption of the fetuses. In fact, several of the $p53^{C/C(ESC)}$ chimeras with normal body size displayed increased number of apoptotic cells in the liver (Fig. 3h, arrowheads) and one chimera exhibited an abnormal spinal curvature (Fig. 3i, an arrow). Embryos such as these may die and undergo resorption before birth, resulting in the significant loss of neonates as shown in Figure 3d.

Morphology and global gene expression profile in $p53^{-/-}$ ESCs. The properties of $p53^{-/-}$ ESCs were examined. Venus-negative differentiated cells (Fig. 4a, left, arrowheads) survived the processes of cloning and passaging $p53^{-/-}$ Venus-positive ESCs (Fig. 4a, left, arrows), indicating that $p53^{-/-}$ differentiated cells escaped from apoptosis. Rat ESC colonies adopt a dome-shaped morphology and tend to detach from culture dishes coated with MEFs[12,15]. The $p53^{-/-}$ domed colonies were detached by pipetting and the cells were passaged after dissociation, leading to successful propagation of dome-shaped colonies; no differentiated cells were detected. (Fig. 4a, right, arrows). The morphology of the $p53^{-/-}$ lines was

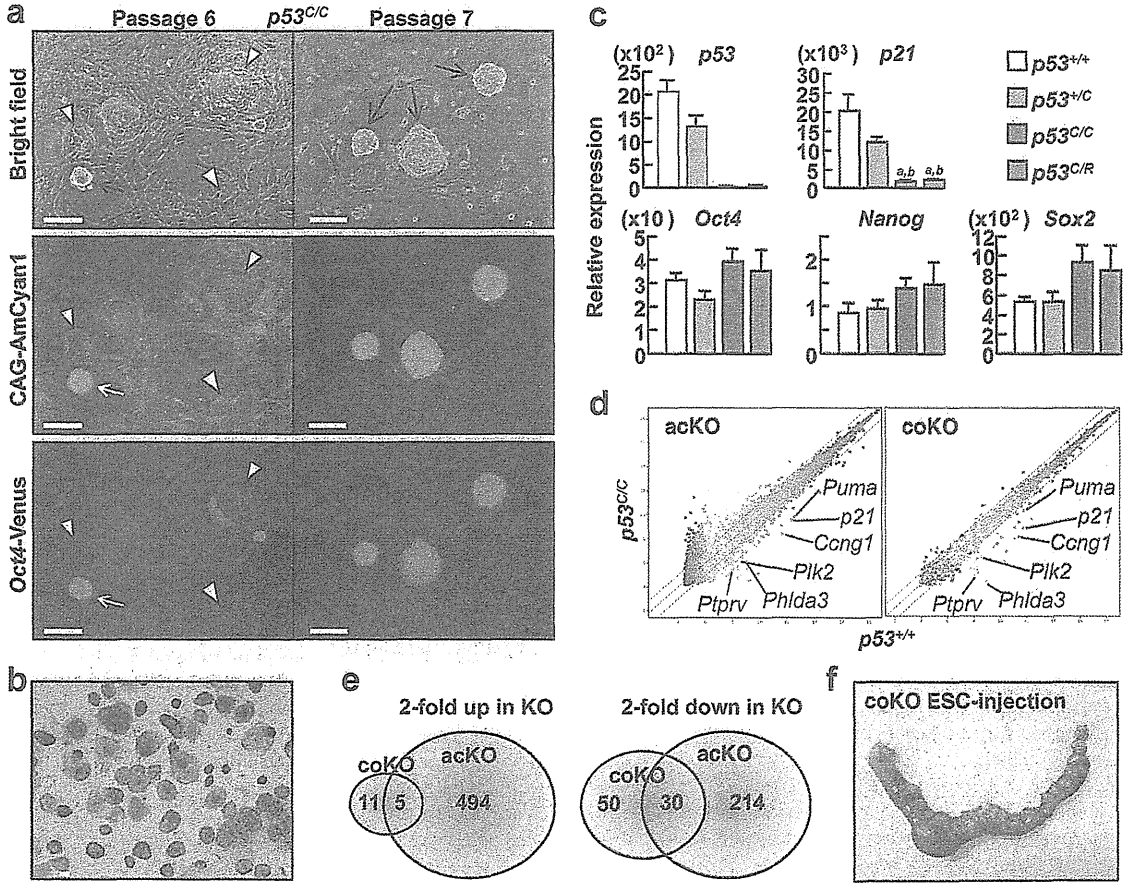

Figure 4 | Characteristics of *p53*-null ESCs. (a) A $p53^{C/C1}$ ESC clone is shown. Arrows indicate pluripotent colonies. Arrowheads indicate differentiated cells. (b) ALP staining in $p53^{C/C1}$ ESCs. (c) q-PCR analysis in *p53* mutant ESCs. Transcript levels were normalized to *Gapdh* levels. Data are the mean ± SD of one biological sample assayed in four independent experiments. *a*, $P<0.05$ versus $p53^{+/+}$; *b*, $P<0.005$ versus $p53^{+/C}$. (d) Scatter plots of global gene expression microarrays comparing $p53^{+/+}$ and $p53^{C/C}$ ESCs of an acKO (left) or coKO (right) line. The green lines delineate the boundaries of a 2-fold difference in gene expression levels. (e) Venn diagrams of the intersection between genes highly (left) or lowly (right) expressed in the coKO versus the acKO in $p53^{C/C}$ ESCs. (f) Developmental dysfunction in chimeric embryos injected with $p53^{C/C2}$ coKO ESCs at E16.0. All scale bars = 100 μm.

indistinguishable from that of $p53^{+/-}$ or $p53^{+/+}$ cells (Supplementary Fig. S3). The $p53^{C/C}$ ESCs were positive for alkaline phosphatase (ALP) activity (Fig. 4b).

The expression levels of ESC marker genes, such as *Oct4*, *Nanog* and *Sox2*, were similar in $p53^{C/C}$ and $p53^{C/R}$ ESCs compared to $p53^{+/+}$ or $p53^{+/C}$ cells, whereas loss of *p53* mRNA and parallel reduction in the mRNA level of the *p53* target gene *p21* were confirmed in mutant ESC lines (Fig. 4c). The ESC line produced by acquired gene targeting in wild-type ESCs ('acKO' ESCs) and a congenital KO ESC line derived from heterozygous intercrosses (named coKO) were analyzed to determine whether some compensatory effect occurred in the coKO line. A microarray analysis showed that the coKO line had less divergent expression compared to the acKO line (acKO vs. coKO: 494 vs. 11 genes upregulated and 214 vs. 50 genes downregulated, Fig. 4e). Venn diagrams showing the overlap in genes identified in the two KO ESC datasets identified only five upregulated and 30 downregulated genes (Fig. 4e, and see Supplementary Table S2). Many of the downregulated genes in the $p53^{C/C}$ ESCs were direct targets of *p53*, such as *Puma*, *p21*, *Ccng1*, *Plk2*, *Phlda3*, and *Ptprv* (Fig. 4d), whereas no genes for pluripotency or stemness were identified.

Chimera generation was used to investigate whether microinjection with these coKO ESCs could rescue mutant chimera development. Male ESC lines were also examined because homozygous males showed normal development. However, microinjection of both female cell lines (n=4, 2 cell lines) and male coKO ESC cell lines (n=7, 3 cell lines) produced chimeras in which embryogenesis failed, similar to the acKO chimeras (Fig. 4f and Supplementary Table S1). The fraction of full-sized embryos (15/68 embryos: 23.1 ± 4.0%, n=9, 5 cell lines) was similar to that of acKO chimeras (30/189 embryos: 20.0 ± 5.6%, n=14, 5 cell lines). These results indicate that lethality in mutant chimeras is due to abnormality of $p53^{-/-}$ ESCs.

$p53^{-/-}$ ESCs are resistant to apoptosis and differentiation. To investigate susceptibility to apoptosis, flow cytometry to detect surface exposure of Annexin V was performed in ESCs under routine culture conditions using YPAC medium [Y, Y-27632 (ROCK inhibitor); P, PD0325901 (MEK inhibitor); A, A-83-01 (TGF-β inhibitor); C, CHIR99021 (GSK3 inhibitor)][12]. A control treatment with G418 caused an increase in Annexin V-positive apoptotic cells whereas each of the *p53* genotype ESCs exhibited small population of the apoptotic cells ($p53^{+/+}$, 11.0 ± 0.25%; $p53^{+/C}$, 14.0 ± 0.30%; $p53^{C/C}$, 11.0 ± 0.49%) (Fig. 5a). Assays for colony formation and embryoid body (EB) formation were performed under differentiation culture conditions to examine the behavior of the mutant ESCs. There was no genotype-dependent difference in the numbers of undifferentiated or differentiated colonies under conditions using YPAC medium and MEFs (Fig. 5b). Under culture conditions using Y media and MEFs (inhibitors P, A and C were absent, Fig. 5c), almost no $p53^{+/+}$ undifferentiated colonies formed (1.7 ± 0.9 colonies) but some $p53^{+/C}$ colonies were observed (13.0 ± 2.1 colonies, $P<0.01$). Few differentiated colonies of either genotype were formed. In contrast, $p53^{C/C}$ cells formed a large number of both undifferentiated (56.0 ± 2.6 colonies, $P<0.0001$ vs. $p53^{+/+}$; $P<0.001$ vs. $p53^{+/C}$) and differentiated (26.3 ± 1.5 colonies, $P<0.0001$ vs. $p53^{+/+}$; $P<0.0001$ vs. $p53^{+/C}$) colonies (Fig. 5c). These results suggest that $p53^{-/-}$ ESCs strongly maintain both undifferentiated state and self-renewal capacities while the differentiated cells are protected from apoptosis, consistent with the results shown in Figure 3a. Next, colony formation was assessed under culture conditions in which ESCs weakly attach to un-coated culture dishes in the absence of MEFs. Although undifferentiated colony formation was rare in both $p53^{+/+}$ (11.3 ± 3.5) and $p53^{+/C}$ (2.0 ± 1.2) ESCs, a large number of $p53^{C/C}$ ESCs formed colonies (96.7 ± 2.8 colonies, $P<0.0001$ vs. $p53^{+/+}$; $P<0.0001$ vs. $p53^{+/C}$; Fig. 4d). In the un-coated dishes in the absence of MEFs, differentiated colonies were rarely formed from any ESC genotype. Thus, the $p53^{-/-}$ ESCs might have an increased capacity to adhere tightly to the culture dish and/or proliferate without the support of feeder cells.

When EB formation was examined, $p53^{+/+}$ EBs formed by day 3 underwent apoptosis over time in culture, resulting in few EBs remaining by day 7 relative to day 3. In addition, Venus fluorescence was completely lost in these cells (Fig. 5e, left). In contrast, $p53^{C/C}$ EBs were large in size and number, and maintained Venus fluorescence (Fig. 5e, right). The number of cells in $p53^{C/C}$ EBs (3.25×10^5) was significantly larger than cell number in $p53^{+/+}$ EBs (1.00×10^5, $P<0.01$) or $p53^{+/C}$ EBs (2.47×10^4, $P<0.01$). Moreover, these data indicate that $p53^{C/C}$ EBs actively proliferated because the cell number increased from 2.5×10^5 at day 0 to 3.25×10^5 by day 7 (Fig. 5f). This result suggests that $p53^{C/C}$ cells are able to proliferate even in the absence of cell attachment. $p53^{+/C}$ EBs showed an intermediate phenotype with significant differences from the other genotypes ($P<0.01$ vs. $p53^{+/+}$, $P<0.01$ vs. $p53^{C/C}$).

Chromosomal instability in $p53^{-/-}$ cells. Next, karyotype analysis was performed in $p53^{-/-}$ cells. Although $p53^{+/C}$ ESCs maintained a normal karyotype 42,XX,[20], one $p53^{C/R2}$ ESC clone exhibited abnormal karyotype 42,XX,add(15)(q22)[20] (Fig. 6a, red square and arrow). Moreover, once the $p53^{C/R2}$ ESC clone differentiated under EB forming culture conditions for two weeks (Fig. 6b), an additional chromosomal aberration, 41,X,-X,add(15)(q22)[20], was found in all cells analyzed (Fig. 6a, blue square). In a $p53^{C/C1}$ ESC clone, ESCs did not have an abnormal karyotype (42,XX[20]). However, cells derived from the $p53^{C/C1(ESC)}$ chimera in E14.0 rats displayed various chromosomal aberrations, such as 42,XX,add(1)(q52)[1], 42,XX,add(3)(p12) [1], 43,XX,+16[1] or 42,X,-X,+mar[1]. In cell cultures, $p53^{+/+}$ cells derived from a recipient blastocyst were eliminated, resulting in occupation by $p53^{C/C1}$ cells with AmCyan1 expression (Fig. 6c).

These findings demonstrate that $p53^{-/-}$ ESCs exhibit several features of abnormalities, such as blockage of differentiation, induction of chromosomal instability, and escape from apoptosis, which are facilitated when the cells differentiate. Thus, p53 is indispensable for embryonic development in the mutant chimeric models (Fig. 1f) but dispensable in the homozygous models due to bypassing an ESC state (Fig. 1e).

Discussion

Here, two distinct strategies were used to generate *p53* KO rats: conventionally generated homozygous KO and ESC-based mutant chimeras. In the homozyogous KO rats, NTDs such as exencephaly and spina bifida were observed. This is the first NTD model created in genetically modified rats. Previously, a 50% reduction in the number of females relative to males at weaning was observed in *p53* homozygous KO mice[17]. In contrast, in the present study, a 96% reduction in the number of *p53* homozygous KO female rats surviving to weaning relative to homozygous KO males was observed (Table 1). In rats, exencephaly occurred in a large fraction of the homozygous KO females (55%; Table 1), whereas only 8–16% of homozygous KO female mouse embryos exhibited exencephaly[17,18]. The survival ratio and spina bifida phenotype observed in these exencephalic rat embryos suggests that this species exhibits more severe phenotypes than mice. We hypothesize that rats are more sensitive to the stress of DNA damage than mice. Consistent with this observation, rat ESCs are more sensitive to differentiation signals than mouse ESCs, which is one reason why rat ESCs were not established until 2008. Mouse ESCs are very stable compared to other species. In mouse, successful chimera contribution and germline transmission using *p53*-null mouse iPSCs has been reported[24,25]. These results were unexpected, considering the vast amount of data regarding the effects of p53 on cell cycle arrest, apoptosis, and DNA

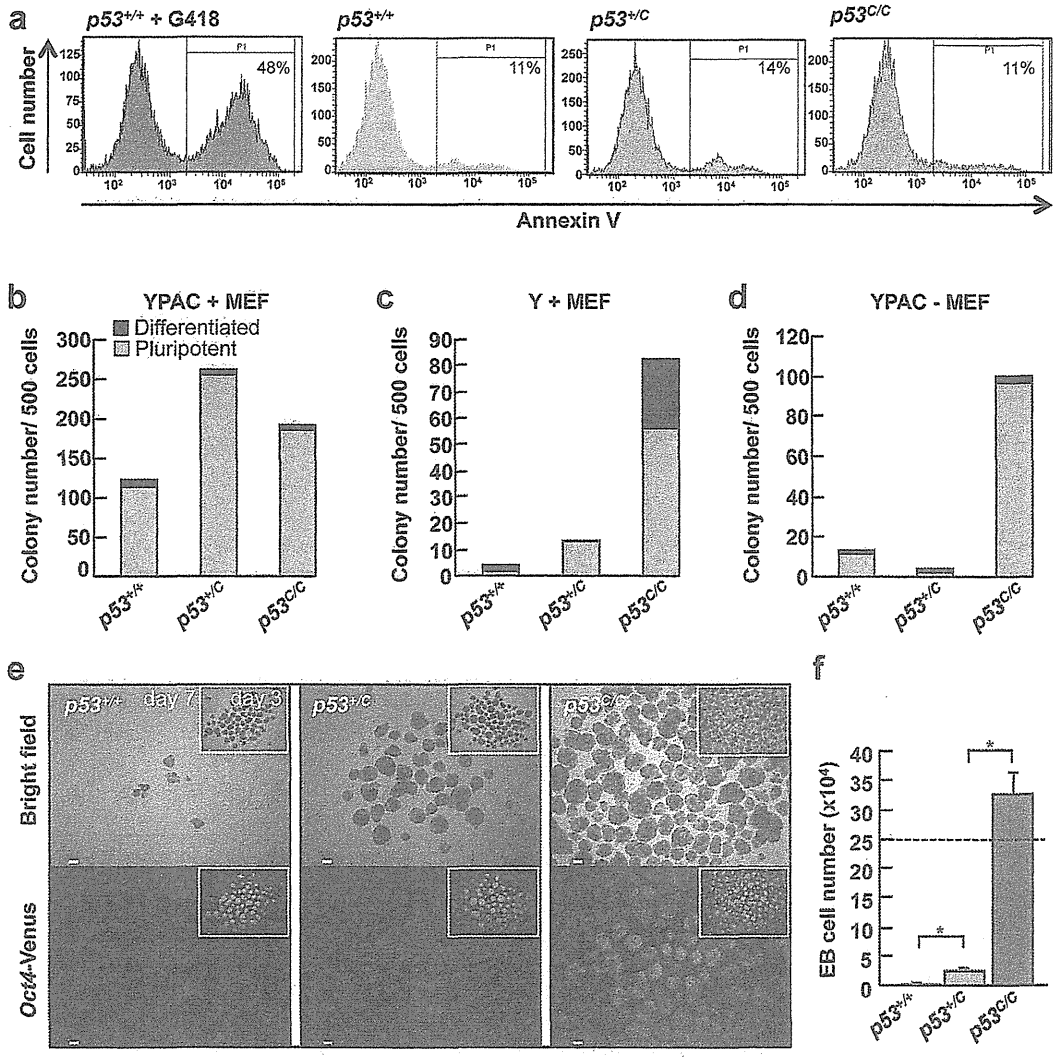

Figure 5 | Colony and EB formation assays under differentiating conditions. (a) Flow cytometry analysis. Annexin V-Cy5 was used to detect apoptotic cells (n=3). (b–d) Colony formation assay. Five hundred cells were cultured under normal conditions (YPAC+MEF; b), differentiation conditions (Y+MEF; c), or apoptosis-inducing conditions (YPAC-MEF; d). A green or black bar indicates pluripotent or differentiated colony number, respectively (n=3 or 4). (e, f) EB formation assay. EBs were formed from 2.5×10^5 cells (f, dotted line). Seven days after incubation without inhibitors, the cell number was counted (f, n=3). Insets (e) indicate EBs at day 3. *, $P < 0.01$. All scale bars = 100 μm.

repair. In contrast, in the present study, mutant chimeras generated with rat ESCs demonstrated a clear phenotype of embryonic lethality, consistent with the data presented here showing the down-regulation of *p53* target genes, inhibition of apoptosis and differentiation, and increase in chromosomal instability in *p53*-null rat ESCs or ESC-derived cells.

The rat is considered to be a better model than the mouse for many complex disorders that are common in humans[36] and is currently the primary animal model in many preclinical tests, especially those related to cardiovascular disease, diabetes, breast cancer, chronic inflammatory diseases, and age-related diseases[20]. Genetically modified rats are valuable platforms for the study of human physiology and disease. For example, in comparison to transgenic mice, transgenic rat models of Huntington disease not only present a more typical adult patient pathology but are also more suitable for *in vivo* metabolic and structural imaging[20,37]. In addition, *Apc* knockout mice develop tumors primarily in the small intestine, whereas both humans and rats develop colon cancer as a result of the *Apc* mutation[38]. These observations support the inconsistent phenotype of *p53* mutant chimeras between rats and mice, as shown in the present work, and suggest the importance of generating genetically modified rats to find novel gene functions.

In this study, the differences in the phenotypes of the *p53* homozygous and mutant chimeric rat models were striking. Secondary mutations are accumulated in the mutant ESCs under *in vitro* culture conditions and in the differentiating cells during embryogenesis (Fig. 6). These aberrant cells are resistant to apoptosis due to *p53* deficiency, which might lead to lethality of the mutant chimeras. These observations reflect the fact that a major p53 function is to be the "guardian of the genome". Thus, the mutant chimeric strategy may prove useful in identifying authentic and/or novel gene functions. Finally, the present study demonstrated that mutant chimeric models can be generated within one month, circumventing both the risks associated with producing successful germline transmission as well as the time frame required for breeding both chimeras and heterozygous animals. In the mutant chimeric method, double or triple gene knockouts can be generated in a few months. These new combination strategies using embryonic stem cells, the mutant

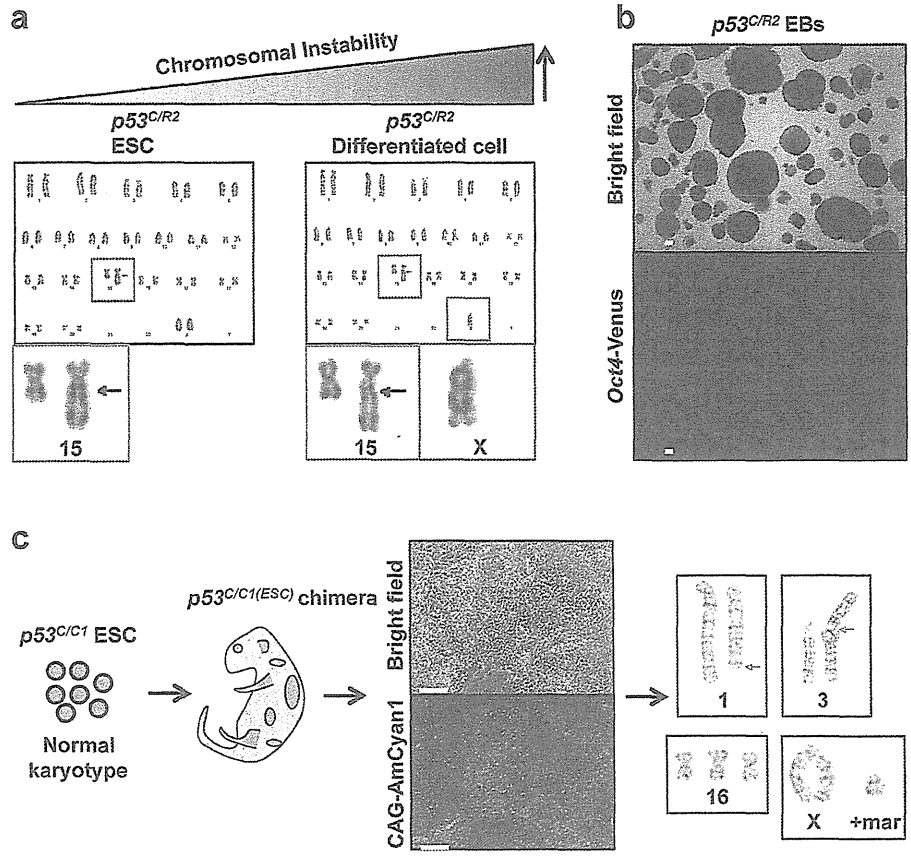

Figure 6 | **Chromosomal instability in *p53*-null cells.** (a) Cytogenetic analysis by G-band staining in $p53^{C/R2}$ ESCs and EB-derived differentiated $p53^{C/R2}$ cells. Abnormal chromosomes were indicated by red and blue squares. (b) Differentiated $p53^{C/R2}$ EBs lacking Venus fluorescence. (c) Aberrant chromosomes were observed in cells derived from a $p53^{C/C1(ESC)}$ chimera at E14.0.

chimeric method, and rats instead of mice will provide great insight into the novel functions of a large number of genes. The first example, shown here by deleting the *p53* gene, provided new, substantial evidence demonstrating that p53 functions not only as the "guardian of the genome", but also as the "guardian of the embryogenesis".

Methods

Media, feeder cells, animals, and primers. The YPAC medium was prepared by the addition of the following inhibitors: 10 μM Y-27632 (WAKO), 1 μM PD0325901 (Axon Medchem), 0.5 μM A-83-01 (TOCRIS), and 3 μM CHIR99021 (Axon Medchem) to a basic medium. The basic medium was composed of DMEM (including 110 mg/L sodium pyruvate and 200 mM GlutaMAX, GIBCO), 20% FBS (ES Cell Qualified Fetal Bovine Serum, Lot No. 1204059, GIBCO), 0.1 mM 2-mercaptoethanol (SIGMA), 1% nonessential amino acid stock (GIBCO), and 1× antibiotic antimycotic (GIBCO). Mitomycin C-treated MEFs resistant to neomycin (Millipore) were used as feeders and maintained in 10% FBS DMEM (Lot No. SFB30-1502, EQUITECH-BIO, INC.) with 1× antibiotic antimycotic. Animal experiments were performed in compliance with the guidelines of the Institute for Laboratory Animal Research, National Cancer Center Research Institute. These studies were approved by National Cancer Center Research Institute. All primer sequences are listed in Supplementary Table 3.

Generation of *Oct4*-Venus Tg rats and ESCs. *Oct4*-Venus Tg rats of the Wistar strain were generated via germline transmission of an *Oct4*-Venus ESC clone in the same manner described previously[12]. The *Oct4*-Venus ESC line derived from the Long-Evans Agouti (LEA) strain was generated in an earlier study[12].

Establishment of rat ES cells from blastocysts. Rat blastocysts were gently flushed out from the uteri of E4.5 or E5.0 pregnant rats with a basic ES medium. After removal of the zona with acid Tyrode's solution (Ark Resource Co., Ltd.), whole blastocysts were plated onto 6-well plates and cultured on MEFs in basic ES medium with or without YPAC. After approximately 7 days, the blastocyst outgrowths were cut into pieces and replated under the same YPAC conditions. Emerging ESC colonies were then dissociated with Accutase (Innovative Cell Technologies, Inc.) and expanded. Domed and floated ESC colonies were detached from MEFs by pipetting, followed by routinely passaging every 3–4 days under MEF-YPAC conditions.

ZFN constructs and targeting plasmids. Custom-designed ZFN plasmids and ZFN-encoding mRNA for the rat *p53* gene were purchased from Sigma-Aldrich. The design, cloning, and validation of the ZFNs were performed by Sigma-Aldrich. The ZFN pair recognizing exon 4 of the *p53* gene was 5′: TTCTCCAGTCTTCCTCCAG, 3′: ATTCTGGTAAGGAGCCGG. The targeting donor was composed of the CAG-AmCyan1-IRES-Neo-pA or CAG-tdTomato-IRES-Neo-pA cassette with short homology 5′ (736 bp) and 3′ (711 bp) arms. These homology arms were amplified from rat genomic DNA using the KOD Ver.2 DNA polymerase PCR system (Toyobo). The sequences of these primers are listed in Supplementary Table S3. Both arms were set at several base pairs from a ZFN-induced cleavage site.

Introduction of the targeting vector and ZFNs into LEA rat ESCs and generation of *p53* heterozygous rats. To disrupt exon 4 of the *p53* gene, 5 μg of ZFN-encoding mRNAs and 10 μg of a targeting plasmid (5′arm-CAG-AmCyan1-IRES-Neo-pA-3′arm cassette) were co-transfected into 6.5×10^5 of *Oct4*-Venus ESCs derived from a LEA female strain at passage 5 with a Mouse ESC Nucleofector Kit (Amaxa Inc.). The cells were plated on MEFs in YPAC medium with 2% Matrigel (BD Biosciences) to keep the ESC colonies adhered to the MEFs. One day after nucleofection, geneticin was added to the YPAC medium at 0.2 μg/ml. Eleven days after nucleofection, geneticin-resistant colonies were selected using handmade capillaries and expanded. Picking and expanding seven colonies provided four (57%) heterozygous ($p53^{+/C}$) clones and two (29%) homozygous clones harboring both knock-in and frame shift mutation alleles ($p53^{C/2}$) (Supplementary Fig. S1a). The ZFN-induced frame shift mutation was identified by band shift in PCR analysis (Supplementary Fig. S1a, No. 6 clone, asterisk) and sequence analysis (Supplementary Fig. S1c) or using a SURVEYOR Mutation Detection Kit (Supplementary Fig. S1b, No. 8 clone). A $p53^{+/C}$ ESC clone was used for microinjection, resulting in the generation of $p53^{+/C}$ rats through chimeric germline transmission.

Introduction of the targeting vector and ZFNs into Wistar rat ESCs. For nucleofection, 10 μg of a targeting plasmid (5′arm-CAG-AmCyan1-IRES-Neo-pA-3′arm

cassette) and 5 μg of ZFN-encoding mRNAs were co-transfected into 4.5×10^6 of *Oct4*-Venus ESCs (Wistar) at passage 3. As a control experiment, 10 μg of the targeting plasmid without ZFNs was transfected into 4.5×10^6 of *Oct4*-Venus ESCs at passage 3. One out of 46 (2.2%) clones was $p53^{C/C}$, while seven of 46 (15%) clones were $p53^{C/Z}$. A sequence data revealed an 8-bp deletion in the $p53^{C/Z1}$ clone (Figure S2B). This ZFN-induced small deletion was also confirmed by a downward band shift (indicated by asterisks in Supplementary Fig. S2a). As a control experiment, the targeting vector alone was introduced without ZFN. Although 14 geneticin-resistant colonies appeared, they did not achieve homologous recombination (Supplementary Fig. S2a, lane 5). Knockout clones were also produced using a 2nd-step recombination by introducing the 10 μg of targeting plasmid (5′arm-CAG-tdTomato-IRES-Neo-pA-3′arm cassette) and 5 μg of ZFN-encoding mRNAs into 2.5×10^6 cells of a $p53^{+/C3}$ ESC clone at passage 9 (Fig. 6). Eight red fluorescence (tdTomato)-positive clones were chosen without geneticin selection, and successful homologous recombination was achieved in three of these (38%, $p53^{C/R}$; Supplementary Fig. S2c).

Surveyor nuclease (Cel-I) assay. A ZFN target locus was amplified by PCR (35 cycles: 10 s denaturing at 98°C, 30 s annealing at 62°C and 1 min elongation at 72°C) using primers 1 and 5 (Fig. 6 and Supplementary Table S3). The Cel-I assay was carried out following the manufacturer's protocol (TRANSGENOMIC, Inc.).

ALP staining, immunohistochemistry (IHC) and Annexin V-apoptosis assay. Cells were fixed in 4% paraformaldehyde. ALP staining was performed with the Vector Blue substrate (Vector Labs) according to the manufacturer's instructions. Formalin-fixed and paraffin-embedded slides were stained with hematoxylin and eosin or used for IHC. Antigen retrieval was performed by autoclave in a sodium citrate buffer. The slides were incubated with Sox2 (BioLegend, 1 : 200) or Cleaved Caspase-3 (Cell Signaling, 1/1000) primary antibody at 4°C overnight. The next day, after washing, the samples were incubated with horseradish peroxidase-conjugated secondary antibody for 1 h. They were then washed and incubated with 3,3′-diaminobenzidine tetrahydrochloride DAB (Thermo Scientific). An assay for apoptotic ESCs was performed using Annexin V-Cy5 following the manufacturer's protocol (BioVision). Pluripotent ESC colonies were solely harvested and dissociated with Accutase, followed by incubating $1–5 \times 10^5$ cells with the Annexin V-Cy5 for 5 min in the dark.

Q-PCR analysis. Total RNA was isolated using ISOGEN (Nippongene). cDNA was synthesized with 2 μg of the total RNA using Super Script III RT (Invitrogen) and oligo-dT primer (Invitrogen). cDNAs were used for PCR using Platinum SYBR Green qPCR SuperMix UDG (Invitrogen). Optimization of the q-PCR reaction was performed according to the manufacturer's instructions (PE Applied Biosystems, Tokyo, Japan). All quantitations were normalized to an endogenous control *GAPDH*.

Microarray analysis. A one-color microarray-based gene expression analysis system (Agilent Technologies) using SurePrint G3 Rat GE 8×60 K Kit containing 30507 probes (26930 genes) was used following the manufacturer's instructions.

EB formation. After ES cells were dissociated into single cells using Accutase, 5×10^5 cells were cultured in PAC medium. After overnight incubation, the EB contained media were separated and cultured in media with or without PAC on a low cell-binding dish (NUNC). After 7 days of incubation, the cell number of EBs was counted after dissociation with Accutase.

Chimera production. In all blastocyst injection experiments, 12 ESCs were injected into E4.5 blastocysts. YPAC or PAC inhibitors were constantly included in media during both microinjection and blastocyst incubation. ESC-injected blastocysts were transferred to E3.5 pseudo-pregnant rats. The contribution of ESCs to the resulting chimeras was determined by the appearance of coat-color or fluorescence.

Karyotype analyses in $p53^{-/-}$ cells. G-band staining was performed in cultured cells from embryos, ESCs, or ESC-derived differentiated cells. Head of E14.0 chimeric embryo was dissociated with Accutase and karyotype analysis was examined in the cells at passage 4. $p53^{C/R2}$ ESCs at five passages after the generation of the gene-targeted null mutation or EB-derived differentiated $p53^{C/R2}$ cells at seven passages were analyzed. EBs were formed at passage 5 and cultured for 2 weeks, followed by two passages to expand the cells. The differentiated state was confirmed by a loss of *Oct4*-Venus expression, as well as by the cell morphology.

Statistical analysis. Results are given as the mean ± SD. Statistical analysis was conducted using Student *t*-tests. $P < 0.05$ was considered significant.

1. Cozzi, J. *et al.* Pronuclear DNA injection for the production of transgenic rats. *Methods Mol. Biol.* **561**, 73–88 (2009).
2. Dann, C. T., Alvarado, A. L., Hammer, R. E. & Garbers, D. L. Heritable and stable gene knockdown in rats. *Proc. Natl. Acad. Sci. U S A.* **103**, 11246–11251 (2006).
3. Zan, Y. *et al.* Production of knockout rats using ENU mutagenesis and a yeast-based screening assay. *Nat. Biotechnol.* **21**, 645–651 (2003).
4. van Boxtel, R., Gould, M. N., Cuppen, E. & Smits, B. M. ENU mutagenesis to generate genetically modified rat models. *Methods Mol. Biol.* **597**, 151–167 (2010).
5. Kitada, K. *et al.* Transposon-tagged mutagenesis in the rat. *Nat. Methods* **4**, 131–133 (2007).
6. Kitada, K., Keng, V. W., Takeda, J. & Horie, K. Generating mutant rats using the Sleeping Beauty transposon system. *Methods* **49**, 236–242 (2009).
7. Izsvák, Z. *et al.* Generating knockout rats by transposon mutagenesis in spermatogonial stem cells. *Nat. Methods* **7**, 443–445 (2010).
8. Geurts, A. M. *et al.* Knockout rats via embryo microinjection of zinc-finger nucleases. *Science* **325**, 433 (2009).
9. Mashimo, T. *et al.* Generation of knockout rats with X-linked severe combined immunodeficiency (X-SCID) using zinc-finger nucleases. *PLoS One* **5**, e8870 (2010).
10. Buehr, M. *et al.* Capture of authentic embryonic stem cells from rat blastocysts. *Cell* **135**, 1287–1298 (2008).
11. Li, P. *et al.* Germline competent embryonic stem cells derived from rat blastocysts. *Cell* **135**, 1299–1310 (2008).
12. Kawamata, M. & Ochiya, T. Generation of genetically modified rats from embryonic stem cells. *Proc. Natl. Acad. Sci. USA* **107**, 14223–14228 (2010).
13. Hamanaka, S. *et al.* Generation of germline-competent rat induced pluripotent stem cells. *PLoS One* **6**, e22008 (2011).
14. Hirabayashi, M. *et al.* Rat transgenesis via embryonic stem cells electroporated with the Kusabira-orange gene. *Mol. Reprod. Dev.* **77**, 474 (2010).
15. Tong, C., Li, P., Wu, N. L., Yan, Y. & Ying, Q. L. Production of p53 gene knockout rats by homologous recombination in embryonic stem cells. *Nature* **467**, 211–213 (2010).
16. Donehower, L. A. *et al.* Mice deficient for p53 are developmentally normal but susceptible to spontaneous tumours. *Nature* **356**, 215–221 (1992).
17. Armstrong, J. F., Kaufman, M. H., Harrison, D. J. & Clarke, A. R. High-frequency developmental abnormalities in p53-deficient mice. *Curr. Biol.* **5**, 931–936 (1995).
18. Sah, V. P. *et al.* A subset of p53-deficient embryos exhibit exencephaly. *Nat. Genet.* **10**, 175–180 (1995).
19. Donehower, L. A. & Lozano, G. 20 years studying p53 functions in genetically engineered mice. *Nat. Rev. Cancer* **9**, 831–841 (2009).
20. Huang, G. *et al.* Beyond knockout rats: new insights into finer genome manipulation in rats. *Cell Cycle* **10**, 1059–1066 (2011).
21. van Boxtel, R. *et al.* Homozygous and heterozygous p53 knockout rats develop metastasizing sarcomas with high frequency. *Am. J. Pathol.* **179**, 1616–1622 (2011).
22. Puzio-Kuter, A. M. & Levine, A. J. Stem cell biology meets p53. *Nat. Biotechnol.* **27**, 914–915 (2009).
23. Lin, T. *et al.* p53 induces differentiation of mouse embryonic stem cells by suppressing Nanog expression. *Nat. Cell Biol.* **7**, 165–171 (2005).
24. Hong *et al.* Suppression of induced pluripotent stem cell generation by the p53–p21 pathway. *Nature* **460**, 1132–1135 (2009).
25. Marion *et al.* A p53-mediated DNA damage response limits reprogramming to ensure iPS cell genomic integrity. *Nature* **460**, 1149–1153 (2009).
26. Kawamata, M. & Ochiya, T. Establishment of embryonic stem cells from rat blastocysts. *Methods Mol. Biol.* **597**, 169–177 (2010).
27. Kawamata, M. & Ochiya, T. Gene-manipulated embryonic stem cells for rat transgenesis. *Cell Mol. Life Sci.* **68**, 1911–1915 (2011).
28. Hosako, H. *et al.* The roles of p53 and p21 in normal development and hyperthermia-induced malformations. *Birth Defects Res. B Dev. Reprod. Toxicol.* **86**, 40–47 (2009).
29. Chen, X. *et al.* Sex difference in neural tube defects in p53-null mice is caused by differences in the complement of X not Y genes. *Dev. Neurobiol.* **68**, 265–273 (2008).
30. Takemoto, T. *et al.* Tbx6-dependent Sox2 regulation determines neural or mesodermal fate in axial stem cells. *Nature* **470**, 394–398 (2011).
31. Miyagi, S. *et al.* The Sox2 regulatory region 2 functions as a neural stem cell-specific enhancer in the telencephalon. *J. Biol. Chem.* **281**, 13374–13381 (2006).
32. Hockemeyer, D. *et al.* Efficient targeting of expressed and silent genes in human ESCs and iPSCs using zinc-finger nucleases. *Nat. Biotechnol.* **27**, 851–857 (2009).
33. Soldner, F. *et al.* Generation of Isogenic Pluripotent Stem Cells Differing Exclusively at Two Early Onset Parkinson Point Mutations. *Cell* **146**, 318–331 (2011).
34. Meyer, M., de Angelis, M. H., Wurst, W. & Kühn, R. Gene targeting by homologous recombination in mouse zygotes mediated by zinc-finger nucleases. *Proc. Natl. Acad. Sci. USA* **107**, 15022–15026 (2010).
35. Cui, X. *et al.* Targeted integration in rat and mouse embryos with zinc-finger nucleases. *Nat. Biotechnol.* **29**, 64–67 (2011).
36. Abbott, A. Return to the rat. *Nature* **460**, 788 (2009).
37. von Horsten, S. *et al.* Transgenic rat model of Huntington's disease. *Hum. Mol. Genet.* **12**, 617–24 (2003).
38. Amos-Landgraf, J. M. *et al.* A target-selected Apc-mutant rat kindred enhances the modeling of familial human colon cancer. *Proc. Natl. Acad. Sci. U.S.A.* **104**, 4036–41 (2007).

Acknowledgements

We thank F. Takeshita, T. Katsuda, K. Hagiwara, Y. Yoshioka, R. Takahashi, N. Kosaka, H. Tsuda, H. Sasaki and Y. Tamai for their technical advice. This work is supported by a Grant-in-Aid from the Third-Term Comprehensive 10-Year Strategy for Cancer Control.

Author contributions

M.K. designed and performed experiments. M.K. and T.O. wrote the manuscript. T.O. supervised the project.

Additional information

Supplementary information accompanies this paper at http://www.nature.com/scientificreports

Competing financial interests: The authors declare no competing financial interests.

How to cite this article: Kawamata, M. & Ochiya, T. Two distinct knockout approaches highlight a critical role for p53 in rat development. *Sci. Rep.* 2, 945; DOI:10.1038/srep00945 (2012).

STEM CELLS®
CANCER STEM CELLS

LGR5-Positive Colon Cancer Stem Cells Interconvert with Drug-Resistant LGR5-Negative Cells and Are Capable of Tumor Reconstitution

SHINTA KOBAYASHI,[a,b] HISAFUMI YAMADA-OKABE,[b] MASAMI SUZUKI,[b] OSAMU NATORI,[a,b] ATSUHIKO KATO,[b] KOICHI MATSUBARA,[a,b] YU JAU CHEN,[a] MASAKI YAMAZAKI,[b] SHINICHI FUNAHASHI,[c] KENJI YOSHIDA,[c] ERI HASHIMOTO,[d] YOSHINORI WATANABE,[d] HIRONORI MUTOH,[d] MOTOOKI ASHIHARA,[d] CHIE KATO,[b] TAKESHI WATANABE,[b] TAKASHI YOSHIKUBO,[b] NORIKAZU TAMAOKI,[e] TAKAHIRO OCHIYA,[f] MASAHIKO KURODA,[g] ARNOLD J. LEVINE,[h] TATSUMI YAMAZAKI[c,i]

[a]PharmaLogicals Research Pte. Ltd., Singapore; [b]Gotemba Research Laboratories, Chugai Pharmaceutical Co., Ltd., Japan; [c]Forerunner Pharma Research Co., Ltd., Japan; [d]Kamakura Research Laboratories, Chugai Pharmaceutical Co., Ltd., Japan; [e]Central Institute for Experimental Animals, Kawasaki, Japan; [f]Division of Molecular and Cellular Medicine, National Cancer Center Research Institute, Tokyo, Japan; [g]Department of Molecular Pathology, Tokyo Medical University, Tokyo, Japan; [h]Institute for Advanced Study, Princeton, New Jersey, USA; [i]Chugai Pharmaceutical Co., Ltd., Japan

Key Words. Cancer stem cells • Drug target • Experimental models • Monoclonal antibodies • Colon cancer • LGR5

ABSTRACT

The cancer stem cell (CSC) concept has been proposed as an attractive theory to explain cancer development, and CSCs themselves have been considered as targets for the development of diagnostics and therapeutics. However, many unanswered questions concerning the existence of slow cycling/quiescent, drug-resistant CSCs remain. Here we report the establishment of colon cancer CSC lines, interconversion of the CSCs between a proliferating and a drug-resistant state, and reconstitution of tumor hierarchy from the CSCs. Stable cell lines having CSC properties were established from human colon cancer after serial passages in NOD/Shi-*scid*, IL-2Rγ^{null} (NOG) mice and subsequent adherent cell culture of these tumors. By generating specific antibodies against LGR5, we demonstrated that these cells expressed LGR5 and underwent self-renewal using symmetrical divisions. Upon exposure to irinotecan, the LGR5$^+$ cells transitioned into an LGR5$^-$ drug-resistant state. The LGR5$^-$ cells converted to an LGR5$^+$ state in the absence of the drug. DNA microarray analysis and immunohistochemistry demonstrated that HLA-DMA was specifically expressed in drug-resistant LGR5$^-$ cells, and epiregulin was expressed in both LGR5$^+$ and drug-resistant LGR5$^-$ cells. Both cells sustained tumor initiating activity in NOG mice, giving rise to a tumor tissue hierarchy. In addition, anti-epiregulin antibody was found to be efficacious in a metastatic model. Both LGR5$^+$ and LGR5$^-$ cells were detected in the tumor tissues of colon cancer patients. The results provide new biological insights into drug resistance of CSCs and new therapeutic options for cancer treatment. STEM CELLS *2012;30:2631–2644*

Disclosure of potential conflicts of interest is found at the end of this article.

INTRODUCTION

Tumors arise from normal tissues by the progression of multiple mutations resulting in malignant cells. The origin of the cells harboring these mutations, whether stem cells (SCs), progenitor cells, or mature differentiated cells, remains unclear. The heterogeneity of tumor cell types and the prevalence of drug resistance have led to the hypothesis for the existence of cancer stem cells (CSCs), although this theory is still an ongoing debate [1–7].

Evidence for the existence of colon CSCs has been the most convincing, with LGR5-positive (LGR5$^+$) cells of particular interest in CSC studies [8–12]. Lgr5, a Wnt target gene, was first identified as a marker for normal SCs in the intestine [13]. It was also reported that Lgr5-positive (Lgr5$^+$) cells formed adenomas upon deletion of Apc and that Lgr5 is expressed in colon cancer cell lines [8]. The cells with high

Authors contributions: H.Y.O and T. Yamazaki: conception and design, data analysis and interpretation, and writing manuscript, and final approval of manuscript; S.K., M.S., O.N., A.K., K.M., and T.O.: collection and assembly of data and data analysis and interpretation; Y.J.C., M.Y., E.H., Y.W., H.M., M.A., C.K., and T.W.: collection and assembly of data; T. Yoshikubo, N.T., and M.K.: data analysis and interpretation; S.F. and K.Y.: provision of study material (new antibodies); A.J.L.: other (support of manuscript). S. K. and H.Y.O. contributed equally to this article.

Correspondence: Hisafumi Yamada-Okabe, Ph.D., Gotemba Research Laboratories, Chugai Pharmaceutical Co., Ltd., 1-135 Komakado, Gotemba, Shizuoka 412-8513, Japan. Telephone: +81-550-87-6709; Fax: +81-550-87-3637; e-mail: okabehsf@chugai-pharm.co.jp Received April 19, 2012; accepted for publication September 1, 2012; first published online in STEM CELLS *EXPRESS* October 18, 2012. 1066-5099/2012/$30.00/0 doi: 10.1002/stem.1257

Wnt activity, thereby rendering them LGR5$^+$, are functionally designated colon CSCs [14]. Clearly, LGR5 is an important molecule to identify colon CSCs.

In the normal intestine, Tian et al. [15] described that Lgr5-negative (Lgr5$^-$) SCs serve as a reserve population of Lgr5$^+$ cells that are themselves therefore dispensable for normal small intestine cell reproduction. It was also reported that slow cycling SCs positive for Hopx are present at the position 4 (the SC crypt), and that there is an interconversion between Hopx$^+$ slow cycling SCs and Lgr5$^+$ proliferating SCs located at the crypt base [16]. Similarly in CSCs, several reports suggest the existence of distinct states of CSCs [17–21]. However, it remains unknown how proliferating CSCs acquire a drug-resistant phenotype and whether interconversion between proliferating and slow cycling/quiescent CSCs occurs. Difficulties in investigating CSCs are due to the heterogeneity of cell types and the rare presence of CSCs in cancer tissues. Many attempts have been made to enrich and isolate CSCs by spheroid cultures in vitro, cell sorting with CSC markers, and direct xenotransplantation of cancer cells to immunodeficient mice [22–30]. Although spheroid cultures enrich CSCs, they result in heterogeneous populations of cells and are not efficient enough to isolate and maintain pure CSC populations [14].

Here we report the establishment of human colon cancer cell lines that express LGR5 and possess CSC properties. The cell lines were created using serial passages of colon cancer cells in xenotransplantion in NOD/Shi-*scid*, IL-2Rγ^{null} (NOG) mice followed by adherent culture of cells. For this purpose, we generated antibodies that are specific to LGR5. The obtained LGR5$^+$ cells transitioned to LGR5-negative (LGR5$^-$) cells upon exposure to an anticancer drug, and such LGR5$^-$ cells reverted to LGR5$^+$ cells after re-seeding and culturing without an anticancer drug. By gene expression profiling of the cell lines, we demonstrated that HLA-DMA, which belongs to the HLA class II alpha chain paralogs, is expressed in drug-resistant LGR5$^-$ cells, and epiregulin (EREG), a member of the epidermal growth factor family, which can function as a ligand of epidermal growth factor receptor and most members of the ErbB family of tyrosine-kinase receptors, is expressed in both proliferating LGR5$^+$ and drug-resistant LGR5$^-$ cells. Using antibodies against LGR5, HLA-DMA, and EREG, we show the existence of LGR5$^+$ and LGR5$^-$ cells in xenotransplanted tumor tissues and in human colon cancer tissues from patients. Furthermore, the anti-EREG antibody exhibited antitumor activity against tumors derived from the LGR5$^+$ cells in a metastatic model. This is the first demonstration of the establishment of stable cell lines having CSC properties and the ability to transition between the two distinct states, a proliferating and a drug-resistant state. Thus, LGR5$^+$ colon CSCs interconvert with drug-resistant LGR5$^-$ cells and are capable of tumor reconstitution. This suggests the physiological importance of CSCs in tumor recurrence after drug treatment. Further, using the anti-EREG antibody, we provide an option for CSC targeting therapy.

Materials and Methods

Preparation of Monoclonal Antibodies Against LGR5

Anti-LGR5 monoclonal antibodies, 2L36 and 2U2E-2, were obtained by DNA immunization and protein immunization, respectively. For DNA immunization, plasmid DNA containing *LGR5* was transferred once a week six times to the abdominal skin of 6-week-old female MRL/lpr mice (MRL/MpJ-Tnfrsf6<lpr>/Crlj) (Charles River Japan, Yokohama, Japan, http://www.crj.co.jp) using a Helicos Gene Gun (Bio-Rad, Hercules, CA, http://www.bio-rad. com) at a pressure of 200–300 psi. At the final immunization, 1×10^6 cells of CHO DG44 (Life Technologies, Rockville, MD, http://www.lifetech.com) expressing LGR5 were intravenously injected. The splenocytes were resected 3 days after the final immunization and fused with P3-X63-Ag8U1 mouse myeloma cells (ATCC, Manassas, VA, http://www.atcc.org). 2L36 was obtained by screening the culture supernatants of hybridoma by flow cytometry [31].

The N-terminal region of LGR5 (amino acid 1–555) was expressed as a fusion protein with the Fc region of mouse IgG2a in CHO DG44 cell. The LGR5-Fc protein secreted in the culture medium was purified with HiTrap Protein A FF column (GE Healthcare, Little Chalfont, United Kingdom, http://www.gehealthcare.com), and then 6-week-old female BALB/c mice (Charles River Japan) were immunized subcutaneously with 50 μg of the LGR5-Fc protein emulsified in Freund's Complete Adjuvant (Becton Dickinson, Franklin Lakes, NJ, http://www.bd.com). Immunization was repeated once a week for 2 weeks with the same amount of the LGR5-Fc protein in Freund's Incomplete Adjuvant (Becton Dickinson). Three days before cell fusion, mice were injected intravenously with 25 μg of the LGR5-Fc protein. Hybridomas were generated as described above, and the antibody 2U2E-2 was selected by ELISA with the LGR5-Fc protein.

Establishment of Human Colon Cancer Xenografts Using NOG Mice

Colon cancer specimens were obtained from consenting patients, as approved by the ethical committee at PharmaLogicals Research and Parkway Laboratory Services in Singapore. Pieces of tumors were minced by scissors and implanted into the flank of NOG mice (Central Institute for Experimental Animals, Kawasaki, Japan, http://www.ciea.or.jp). The human colon cancer xenografts were maintained by passages in NOG mice. All studies and procedures involving animal subjects were approved by the Animal Care and Use Committee at PharmaLogicals Research and the Institutional Animal Care and Use Committee at Chugai Pharmaceutical Co., Ltd. The animals used in this experiment were treated in accordance with the Animal Research Guideline of PharmaLogicals Research and the Guidelines for the Care and Use of Laboratory Animals at Chugai Pharmaceutical Co., Ltd.

Establishment of Colon Cancer Cell Lines with CSC Properties

Single cell suspension of cancer cells from the xenografts was prepared by mincing the tissues with scissors, incubated in Dulbecco's phosphate buffered saline (DPBS) containing collagenase/dispase (Roche, Basel, Switzerland, http://www.roche-applied-science.com) and DNase I (Roche) at 37°C for 3 hours followed by filtrating 40 μm cell strainer (BD Biosciences, San Diego, CA, http://www.bdbiosciences.com) and suspending in lysing buffer (BD Biosciences). The cells were cultured in a SC medium [Dulbecco's modified Eagle's medium/F12 medium (Life Technologies) supplemented with N-2 supplement (Life Technologies), 20 ng/ml human epidermal growth factor (Life Technologies), 10 ng/ml human basic fibroblast growth factor (Sigma-Aldrich, St. Louis, MO, http://www.sigmaaldrich.com), 4 μg/ml heparin (Sigma-Aldrich), 4 mg/ml bovine serum albumin (BSA) (Life Technologies), 20 μg/ml human insulin, zinc solution (Life

Technologies), and 2.9 mg/ml glucose (Sigma-Aldrich)] at 37°C under 5% CO_2 [32]. Culture flasks treated with polystyrene (BD Biosciences) and ultra-low-attachment cell culture flasks (Corning Life Sciences, Acton, MA, http://www.corning.com/lifesciences) were used for adherent cultures and the spheroid cultures, respectively. Drug-resistant LGR5$^-$ cells were obtained by treating the adherent LGR5$^+$ cells with 10 μg/ml irinotecan (Hospira, Lake Forest, IL, http://www.hospira.com/) for 3 days.

Sorting of the LGR5$^+$ and LGR5$^-$ Cells

The primary cells from xenografts were incubated with the anti-LGR5 antibody (2L36, 2 μg/ml) and then R-phycoerythrin (PE)-labeled anti-mouse IgG2a (Life Technologies, 1/200 dilution). Mouse cells were discriminated from the human colon cancer cells by staining with anti-mouse major histocompatibility complex (MHC) class I antibody (Abcam, Cambridge, U.K., http://www.abcam.com, 0.1 μg/ml) and allophycocyanin (APC)-labeled anti-rat IgG (BioLegend, San Diego, CA, http://www.biolegend.com, 1/100 dilution). Anti-CD133 antibody (Miltenyi Biotec, Bergisch Gladbach, Germany, http://www.miltenyibiotec.com, 5 μg/ml) and Alexa 488-labeled anti-mouse IgG1 (Life Technologies, 1/100 dilution) were used to detect CD133. Dead cells were removed by 7- aminoactinomycin D (7-AAD) viability dye (Beckman Coulter, Brea, CA, http://www.beckmancoulter.com). Flow cytometry analysis and cell sorting were performed using a MoFlo XDP (Beckman Coulter) cell sorter.

In Vitro Colony Formation Assay

To test the colony formation ability, cells were seeded on a layer of 100% Matrigel (BD Biosciences) at 10,000 cells per well and cultured in a SC medium supplemented with 10% heat-inactivated fetal bovine serum (FBS) and 5% Matrigel.

Tumor Formation In Vivo

Cells suspended in Hank's balanced salt solution (Life Technologies) with 50% Matrigel were subcutaneously inoculated into the flank of NOG mice. For single cell inoculation, cells were stained with fluorescein isothiocyanate (FITC)-labeled anti-EpCAM antibody (Miltenyi Biotec) and seeded in Terasaki plates (Thermo Fisher Scientific, Waltham, MA, http://www.thermofisher.com). After the presence of single cell in each well was confirmed under a fluorescence microscope, the single cell in 50 μl of 50% Matrigel was inoculated into the flank of mice. Estimated CSC density was calculated by the formula available on the WEHI ELDA website [33].

Histological Examination

Small pieces of surgical specimens of human tissues and of the xenograft tumor tissues were fixed with 4% paraformaldehyde at 4°C for 16–24 hours and embedded in paraffin by the AMeX method [34, 35]. After washing the in vitro cultured cells with phosphate buffered saline (PBS)-EDTA, the cells were fixed with 4% paraformaldehyde at 4°C for 2 hours, suspended in 0.5 ml agarose, and embedded in paraffin with AMeX method. Thin sections were subjected to hematoxylin & eosin staining and to immunohistochemisty.

Immunohistochemistry

Thin sections from the above-mentioned paraffin blocks were incubated with anti-LGR5 antibody (2U2E-2, 1 μg/ml), anti-EREG antibody (10 μg/ml), anti-E-cadherin antibody (Abcam, 2.5 μg/mL), anti-HLA-DMA antibody (Sigma-Aldrich, 2.5 μg/ml), or FITC-labeled anti-Ki67 antibody (Abcam, 2.5 μg/mL). After the incubation with the primary antibodies, the sections were incubated with a secondary antibody conjugated with polymer-horseradish peroxidase (HRP) (DAKO, Glostrup, Denmark, http://www.dako.com or Vector Laboratories, Burlingame, CA, http://www.vector labs.com) or biotin, and the proteins were visualized by AlexaFluor 488-labeled tyramide (Life Technologies, 1/100 dilution), AlexaFluor 568-labeled tyramide (Life Technologies, 1/100 dilution), or AlexaFluor 568-labeled streptavidin (Life Technologies, 2 μg/ml). For immunofluorescent cytochemistry, cells were fixed with 4% paraformaldehyde and permeabilized with 0.1% Triton-X 100 (Sigma-Aldrich), and incubated with anti-LGR5 antibody (2L36, 2 μg/ml). After the incubation with the primary antibodies, the cells were incubated with AlexaFluor 488-labeled anti-mouse IgG (Life Technologies, 1/100 dilution). Those specimens and cells were also stained with DAPI (Life Technologies).

Induction of the Transition Between LGR5$^+$ and LGR5$^-$ States in Single Cell Culture

LGR5$^+$ cells were sorted with an anti-LGR5 antibody, and single LGR5$^+$ cells were cultured in 96-well microplates. To obtain drug-resistant LGR5$^-$ cells, LGR5$^+$ cells were treated with 10 μg/ml irinotecan for 3 days. Single LGR5$^-$ cells were cultured in 96-well microplates for 4 days. The medium used for the single cell culture contained 10% conditioned medium of the in vitro cultured LGR5$^+$ cells under an adherent condition. LGR5$^+$ and LGR5$^-$ states of the cells were confirmed by immunocytochemical analysis with anti-LGR5 antibody.

Determination of Antitumor Activity of Anti-EREG Antibody In Vivo

2×10^6 of LGR5$^+$ cells were suspended in Hank's balanced sodium solution and intravenously injected into the tail vein of Fox Chase severe combined immunodeficiency (SCID) Beige Mouse (CB17.Cg-Prkdc^{scid}Lyst^{bg}/Crl, Charles River Japan). For treatment with the anti-EREG antibody, the mice were intravenously administered 10 mg/kg of anti-EREG antibody once a week for five times starting 3 days after tumor inoculation. Mice were scarified 5 days after the final administration under deep anesthesia, and lung tissues were collected. The lung tissues trimmed into 11 pieces were fixed in 4% paraformaldehyde for 24 hours, paraffin embedded by AMeX method [34, 35]. After thin sections were prepared and stained with hematoxylin & eosin, the number of tumors was counted. The sizes of the tumors were determined under a microscope with micrometer.

Statistical Analysis

The Mann–Whitney *U* test was applied to determine the statistical significance of the differences in the numbers of tumor nodules in a metastatic tumor model. The statistical analysis was carried out with an SAS preclinical package (SAS Institute, Inc., Cary, NC, http://www.sas.com). *p* values smaller than 0.05 were considered significant.

Results

Generation and Characterization of Specific Antibodies Against LGR5

Having an antibody specific to LGR5 is critical to isolate and characterize colon CSCs, but such antibody has not been available yet. Therefore, we first attempted to generate anti-LGR5 antibodies that enable us to isolate and analyze cells having colon CSC properties. Two monoclonal antibodies, 2L36 and 2U2E-2, specific to LGR5 were obtained. The regions of the LGR5 protein that contain epitopes of these

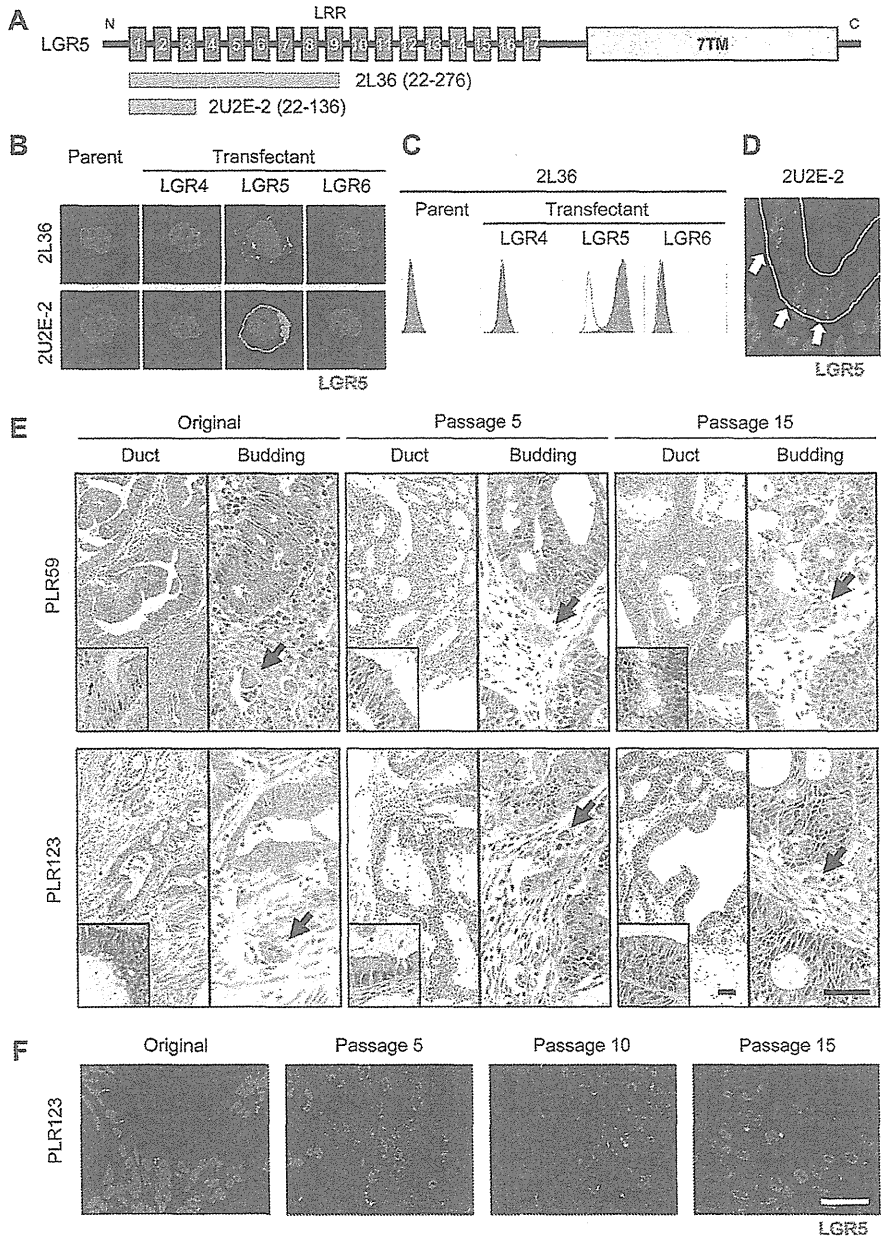

Figure 1. Antigen-specific binding of anti-LGR5 antibodies and characteristics of human colon cancer xenografts using NOG mice. **(A):** Regions of the LGR5 protein that contain epitopes of the anti-human LGR5 monoclonal antibodies, 2L36 and 2U2E-2. The monoclonal antibodies, 2L36 and 2U2E-2, were obtained by immunizing the *LGR5* cDNA and N-terminal region of the protein, respectively. Green bars correspond to the regions containing epitopes. **(B, C):** Specific binding of the anti-LGR5 antibodies to the antigen. (B): Immunocytochemistry of CHO DG44 cells transfected with the *LGR4*, *LGR5*, or *LGR6* cDNA. 2L36 and 2U2E-2 recognized the cells expressing LGR5 but not those expressing LGR4 or LGR6. (C): Flow cytometry analysis of CHO DG44 cells transfected with the *LGR4*, *LGR5*, or *LGR6* cDNA. 2L36 reacted with the cells expressing LGR5 but not those expressing LGR4 or LGR6. **(D):** Staining of the crypt base cells in normal human intestine. The thin sections of the normal human intestine were stained with 2U2E-2. Specific fluorescence was observed in the crypt base columnar cells (arrows). **(E):** Histology of surgically resected tumors of PLR59 and PLR123 and xenograft tumor tissues. Tumors derived from PLR59 and PLR123 had tubular structures containing goblet cells (inserts) and budding cluster (arrows). Bar = 50 μm. **(F):** Immunostaining of LGR5 in the surgically resected tumors (PLR123) and xenografts derived from PLR123. Sections were stained with the anti-LGR5 antibody. Bar = 25 μm. Original, surgically resected tumors from patients.

antibodies are shown in Figure 1A. Both antibodies were tested for immunohistochemistry and flow cytometry using the CHO cells expressing highly related proteins LGR4, LGR5, or LGR6. When used for immunostaining, both 2L36 and 2U2E-2 recognized CHO cells expressing LGR5 but not those expressing LGR4 or LGR6 (Fig. 1B). In flow cytometry analysis, only 2L36 strongly reacted with CHO cells expressing LGR5 (Fig. 1C). Moreover, the antibody 2U2E-2 reacted specifically with crypt base columnar cells in the normal human intestine (Fig. 1D; Supporting Information Fig. S1A).

There was also a good correlation between mRNA expression and cell surface staining of the anti-LGR5 antibody in human colon cancer cell lines, which included the CSC lines established in this study and six commercially available lines (Supporting Information Fig. S1B).

Establishment of Human Colon Cancer Cell Lines with CSC Properties

We established 11 human colon cancer xenografts using NOG mice [36]. Ten out of 11 xenografts were derived from moderately differentiated colon cancer, and one was from poorly differentiated colon cancer. Both the moderately differentiated colon cancer xenografts and the poorly differentiated colon cancer xenograft reconstituted almost the same histological morphologies as the original tumors; the moderately differentiated colon cancer xenografts formed clear epithelial ducts and small budding clusters. In contrast, the poorly differentiated colon cancer xenograft showed no clear epithelial duct structure. We used two moderately differentiated colon cancer xenografts, namely PLR59 and PLR123, for the establishment of colon CSC lines. PLR59 and PLR123 were heterozygous for the mutant K-Ras (G12D), and PLR123 carried the mutant p53 (R249M) in one allele. These xenografts were chosen because they grew faster while retaining the ability to reconstitute tumors with epithelial ducts and small budding clusters even after 10 passages in NOG mice (Fig. 1E). In the epithelial ducts of the tumors, differentiated cancer cells that showed goblet cell-like phenotype were also observed in the xenotransplanted tumor tissues throughout the passages (Fig. 1E, inset).

To confirm the existence of CSCs in the xenotransplanted tumor tissues, we used immunohistochemical staining for the LGR5 protein that marks colon CSCs. LGR5^{+} cells were detected in the original tumor tissues of PLR59 and PLR123 and in their xenotransplanted tumor tissues throughout the passages (Fig. 1F). The frequency of LGR5^{+} cells in the original tumor tissues was quite low: it was approximately 0.01% in PLR59 and approximately 0.04% in PLR123. In the xenotransplanted tumor tissues, the frequency of LGR5^{+} cells increased during the passages (Fig. 1F). Tumor initiating activity (TIA) of the primary cells from the PLR123 xenografts was also increased after the passages. The estimated percentage of CSC in the primary cells, as judged from TIA, was approximately 0.1% after five passages, and after 14 passages it increased to approximately 0.4% (Supporting Information Table S1). Schematic representation of the establishment of the colon cancer cell lines is shown in Figure 2A.

CSC Properties of the Established Colon Cancer Cell Lines

The major properties of CSCs are self-renewal, TIA, and the reconstitution of a tumor tissue hierarchy of differentiated cells. In an attempt to establish cell lines possessing CSC properties, we used spheroid and adherent cultures of the cells derived from PLR59 and PLR123 xenografts in which LGR5^{+} cells were enriched (over 10 passages). When cells derived from PLR59 and PLR123 were cultured as spheroids, their growth was rather slow, and the spheroids contained only a few LGR5^{+} cells but more differentiated cells that were positive for CK20, which is a commonly used differentiation marker (Supporting Information Fig. S2). On the contrary, cells from PLR59 and PLR123 cultured under an adherent condition grew fast with a doubling time of approximately 2.5 days and showed epithelial morphology (Fig. 2B).

To examine TIA of the cells, subcutaneous injection of 10 cells from the spheroids formed tumors in one (PLR59-derived cells) or two (PLR123-derived cells) out of six injection sites (Supporting Information Table S2), whereas 10 cells from adherent cultures formed tumors in all six injection sites, and even a single cell injection of an adherent cell reconstituted tumors. Although the spheroid culture led to an increase in TIA as compared to that of the primary cells, the adherent culture was more efficiently enriched in cells possessing TIA. The histological morphology of the tumors from the adherent cells was almost the same as the original tumors (Fig. 2C). In addition, TIA of the adherent cells was maintained even after the cells were cultured for more than a month (Supporting Information Table S3).

We examined cell surface markers of the adherent cells from the PLR59 and PLR123 and found that they were clearly positive for all known colon CSC markers reported earlier: LGR5^{+}, ALDH^{+}, CD133^{+}, CD44^{+}, EpCAM^{+}, CD166^{+}, CD24^{+}, CD26^{+}, and CD29^{+} (Fig. 2D; Supporting Information Fig. S3). In addition, expression of the cell surface markers was unchanged even after 1 month of cell culture. One of the characteristics of CSCs is symmetrical cell division for self-renewal. The LGR5^{+} adherent cells divided symmetrically under the adherent culture conditions (Fig. 2E). In the presence of Matrigel and FBS, however, the LGR5^{+} cells underwent asymmetrical cell divisions, as demonstrated by the segregation of LGR5 protein into one of two daughter cells (Fig. 2F), implicating the generation of two different offspring. Asymmetric cell divisions are one of the hallmarks of SCs.

Colony Forming Activity and Tumorigenicity of the Sorted LGR5^{+} and the LGR5^{-} Cells

In order to examine the ability of LGR5^{+} and LGR5^{-} cells to form colonies in vitro and tumors in vivo, we sorted the LGR5^{+} and LGR5^{-} populations from the primary cells of xenografts generated by the inoculation of the LGR5^{+} cells. Anti-LGR5 antibody 2L36 was used for the cell sorting. About 93% of the cells in the LGR5^{+} fraction were LGR5^{+}, and more than 99% of the cells in the LGR5^{-} fraction were LGR5^{-} (Fig. 3A). The sorted LGR5^{+} cells but not the LGR5^{-} cells efficiently formed colonies on Matrigel in vitro and formed tumors in NOG mice. When 1,000 cells were subcutaneously injected into NOG mice, the sorted LGR5^{+} cells formed large visible tumors by day 34 after the inoculation, but the LGR5^{-} cells gave rise to only very tiny tumors by day 34 (Fig. 3B). We further examined the relation of LGR5 expression and other CSC markers by double staining the LGR5 with CD133, CD166, or CD44. Nearly all of the LGR5^{+} cells were positive for CD133 and CD166, but there were large numbers of LGR5^{-} cells that were positive for CD133 or CD166, indicating that LGR5 marks a subpopulation of CD133^{+} and CD166^{+} cells (Fig. 3C). Because significant numbers of LGR5^{+}/CD44^{-} cells were present, CD44 does not mark all the LGR5^{+} cells (Fig. 3C).

We used cell sorting to further characterize the LGR5^{-} cell populations. The cells from the xenografts were stained with the anti-LGR5 and anti-CD133 antibodies, and the LGR5^{-}/CD133^{-}, LGR5$^{-/low}$/CD133^{+}, and LGR5^{+}/CD133^{+} cells were separated. More than 90% of the cells in each fraction were LGR5^{-}/CD133^{-}, LGR5$^{-/low}$/CD133^{+}, and LGR5^{+}/CD133^{+} (Fig. 3D). The isolated LGR5^{+}/CD133^{+} and LGR5$^{-/low}$/CD133^{+} cells formed colonies on Matrigel, whereas nearly all the LGR5^{-} /CD133^{-} cells died after seeding on culture plates; colony forming efficiency of the sorted LGR5^{-} /CD133^{-}, LGR5$^{-/low}$/CD133^{+}, and LGR5^{+}/CD133^{+} cells were about 0.03%, 1.6%, and 4.3%, respectively (Fig. 3E; Supporting Information Fig. S4).